January 2013

Self-interference in OFDM-Based Systems: Identification and Separation

Ertugrul Guvenkaya
University of South Florida, eguvenkaya@gmail.com

Self-interference in OFDM-Based Systems: Identification and Separation

by

Ertuğrul Güvenkaya

A thesis submitted in partial fulfillment
of the requirements for the degree of
Master of Science in Electrical Engineering
Department of Electrical Engineering
College of Engineering
University of South Florida

Major Professor: Hüseyin Arslan, Ph.D.
Richard D. Gitlin, Sc.D.
Thomas Weller, Ph.D.

Date of Approval:
March 20, 2013

Keywords: Frequency Domain Eye Diagram, Inter-carrier Interference, Inter-symbol Interference, Interference Identification, Interference Visualization

DEDICATION

To my family.

ACKNOWLEDGMENTS

First, I would like to thank my advisor Dr. Hüseyin Arslan for his guidance, encouragement, and support throughout my study. I wish to thank Dr. Richard D. Gitlin and Dr. Thomas Weller for serving in my committee and for offering valuable suggestions. I hope to be able to benefit from their profound knowledge and experience in the future, as well.

It has been a privilege to have the opportunity to do research as a member of the Wireless Communications and Signal Processing (WCSP) group. I would like to thank my friends Ali Görçin, Alphan Şahin, M. Bahadır Çelebi, Anas Tom, M. Harun Yılmaz, Z. Esad Ankaralı, and Emre Seyyal for their support as friends and productive discussions as colleagues.

Special thanks to Ali Görçin for his sincere support and for everything that I learned from him. Also, I owe much to Yılmaz and Ankaralı families for their great hospitality which minimized the longing to my family and Turkish food.

Last, but by no means least, I would like to express my deepest gratitude to my parents Fatma Güvenkaya, and Yaşar Güvenkaya, and my dear sisters Şüheda and Asude Büşra for their immense sacrifice and their unconditional support throughout the years. It is not possible to thank them enough, but I want them to know that I am grateful to the God for having such a family.

TABLE OF CONTENTS

LIST OF TABLES

LIST OF FIGURES

ABSTRACT

Orthogonal frequency-division multiplexing (OFDM) is communication technique that is robust against multipath spread, efficient in equalization implementation, and flexible in dynamic spectrum usage. With the need of wideband signals in high data rate communications, OFDM has gained widespread attention and usage as an efficient way of implementing multicarrier communication. Despite its prominent advantages, received signal quality degrades because of inter-symbol interference (IS) and inter-carrier interference (ICI) due to insufficient guard time in multipath channels and time variance as well as hardware impairments in OFDM systems. When several of the impairments occurs simultaneously, interferences combine at the receiver side. Thus, interference awareness becomes important concept for OFDM-based systems that are excepted to be highly adaptive for coping with existing impairment. By identifying the type and the source of the interference, mitigation of the impacts with corresponding adaptation in the system increases the performance of the overall system.

In this thesis, self-interference identification, visualization, and separation of various type of interferences in OFDM systems have been studied. An interference spectrogram is developed in order to be able to investigate several interferences with one diagram solely. Identification of different sources of interference that result in same consequences at the receiver, such as ISI due to insufficient guard time and ICI due to time variance in the channel, is performed. Also, powers of corresponding interferences are estimated separately with the proposed technique. Computer simulations and measurements also confirmed the effectiveness of the interference separation method.

Information symbols are represented in various domains of electro space such as time, frequency, and code. Channel impairments have different effects on the symbols in different domains. For instance, multipath spread causes ISI in single carrier systems while interference between symbols occurs when time variance exists in OFDM systems. Visualization and measurement of distortions in various domains need to be addressed for better understanding of multidimensional communication systems and their performance under distortion. Therefore, eye diagram in frequency domain for OFDM-based signals is introduced for visualization and identification of time varying impairments such as frequency spread and carrier frequency offset. Real channel measurements are performed to illustrate the effectiveness of the method in practical cases.

The study conducted in this thesis can be utilized for interference awareness in OFDM-based wireless communication systems. Also, methods and diagrams that are developed can be used for testing the wireless systems, interference measurements, and educational purposes.

CHAPTER 1:

INTRODUCTION

Communication has been one of the fundamental needs of human beings which also lead to the ability to create the language. Besides, by considering smoke signals and beacons, practicing communication wirelessly was introduced before the idea telecommunication. Present understanding of the wireless communication, however, was formed after the experiments of Nicola Tesla [1] that showed the possibility of radio frequency energy transmission and utility for telecommunication of information. After the tremendous developments of the technology, wireless communication has become the most preferred way to connect everything anywhere anytime.

In conventional voice-oriented utilization in communication, data rate requirement does not force the designers in terms of capacity because of the limited bandwidth of the human voice along with moderate increase in the number the users. However, both emerging various data-demanding applications in personal communications and dramatical growth of connected nodes in new areas such as vehicular networking, health monitoring, and smart metering increased the capacity demand in wireless communication systems more than ever.

The need of high capacity translated into the use of broader signal bandwidths throughout decades. Although signal transmission capabilities of the devices supported the wider bandwidths, equalization of the multipath channel limited the practical receiver implementation due to exponential increase in the complexity of the time domain equalization (TDE) as a function of the increase in the multipath delay spread (frequency selectivity) in wideband signal utilization. The limitation of TDE is overcome with another way of equalizing the frequency selective channel: frequency domain equalization (FDE). Alternative to equalization of the multipath channel distortions in time domain, FDE principle provided

reduced computational complexity at the receivers. Efficient discrete Fourier transform (DFT) algorithms [2] paved the way for practical implementation of the equalization by transforming the received signal into the frequency domain, equalizing the signal in this domain, and transforming the equalized signal back into the time domain for demodulation.

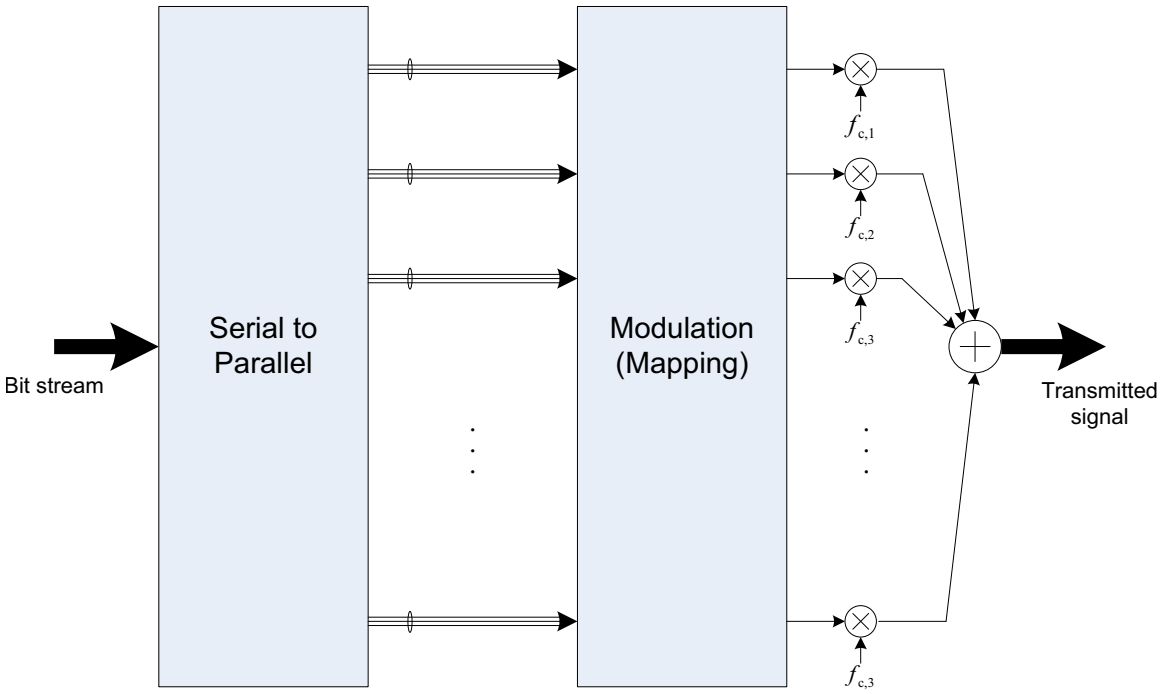

Figure 1.1 Functional block diagram for a simple multicarrier transmitter.

Meanwhile, the idea of multicarrier communication, which had already been introduced at the early sixties [3–6], promised less sensitivity to multipath delay distortions. In multicarrier communication, a wide frequency band is divided into multiple subbands on which the channel has flat frequency response. As illustrated in Figure 1.1, information is parallelly transmitted over narrowband subchannels that gives robustness against delay spread (frequency selectivity) with longer symbol durations.

Orthogonal frequency-division multiplexing (OFDM), which is conventionally referred as multicarrier communication with orthogonal time functions (combination of transmission and reception filters), is a communication technique that can overcome many of the problems that emerge with the high data rate communications, most importantly multipath

delay spread. Although it was not given by Weinstein who introduced the current DFT-based implementation of OFDM [7], conversion of linear convolution of multipath channel response with the signal to circular convolution by inserting cyclic guard time for simple (one tap) FDE has become the enabling factor for OFDM being widely adopted. Then, similar to FDE evolution, efficient OFDM implementation is made posssible with the advances in DFT algorithms. In short, when we say OFDM today, common understanding is a commuication system with successful marriage of DFT-based multicarrier scheme and FDE implementation. More specifically, multicarrier communication scheme with rectangular receiver filter and efficient equalization in the frequency domain as in Figure 1.2. Another factor for the success of OFDM is good accord with multiple input-multiple output (MIMO) systems for increasing the diversity gain and/or enhancing the system capacity [8].

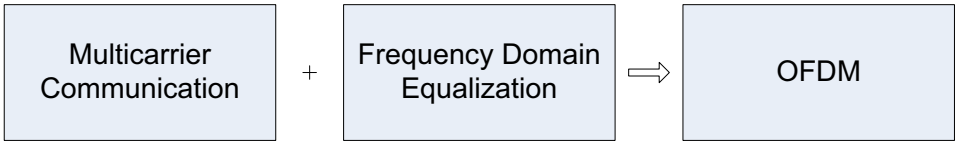

Figure 1.2 OFDM is the communication scheme that combines the advantages of multicarrier communication and frequency domain equalization.

OFDM is used as the modulation method for various communication standards. It is employed in broadcasting schemes such as Digital Audio Broadcasting (DAB) [9] and Terrestrial Digital Video Broadcasting (DVB-T2) [10]. Very-high-speed digital subscriber line 2 (VDSL2) [11] and Broadband over Power Line (BPL) [12] are current examples of wired applications in OFDM for asymmetric digital subscriber line (ADSL)-based and power line communications, respectively. Also, wireless local area network (WLAN) use OFDM as their physical layer (PHY) transmission technique of which the most common example is IEEE 802.11a/g/n family [13]. Success of the OFDM deployment in the WLAN networks encouraged it to be used in metropolitan area networks such as IEEE 802.16 (also known as Worldwide Interoperability for Microwave Access (WiMAX)) [14] and successor

of third generation (3G) cellular systems (fourth generation (4G) cellular) such as Evolved Universal Terrestrial Radio Access (E-UTRA) under the standard organization of 3GPP Long Term Evolution (LTE) [15]. OFDM is also the strongest candidate for cognitive radio (CR) networks for its flexible spectral utilization and efficient implementation as well as the existing knowledge experienced with aforementioned standards [16].

Interference is the limiting factor for quality of the wireless communications. Different from background noise, distortion effect of self-interference on the systems cannot be mitigated by increasing the transmission power because the amount of interference is directly proportional to the signal power itself. As it has been one of the fundamental challenges throughout the history of communication, OFDM also suffers from interference especially when the time variation exists in the channel between transmitter and the receiver. In addition to time varying impairments due to mobility and changes in the environment, misalignment of local oscillators of transmitter and receiver (carrier frequency offset (CFO)), and phase noise at the receiver all of which can be considered under time varying impairments, other problems such as multipath delay spread and time synchronization error create interference between OFDM symbols and subcarriers when utilized guard period is not sufficient. Also, other user's interferences such as narrow band interference (NBI) and adjacent channel interference (ACI) exist in OFDM as one of the strongest candidates for networks adopting opportunistic spectrum usage.

The interference analysis is mainly done by assuming that one type of interference exists in the system. However, both existence and type of the interference source is object to be determined in practical cases to be able to make specific adaptations and countermeasures associated to the existing impairment. For instance, adaptations in guard interval against multipath channels are being considered in both standards [15] and literature [17–19], and subcarrier spacing adaptation techniques have been proposed to maximize the capacity in OFDM-based wireless mobile communication networks [20, 21]. Moreover, multiple impairments can exist at the same time which can occur with high probability in practical scenarios e.g., a highly mobile user along with delay spread longer than the guard period, or multipath delay spread with CFO. In such scenarios, effects of each impairment

combine at the receiver that makes the real cause for degradation of signal quality becomes hard to be detected. Therefore, identification of the interference sources provides insight into the problems in communication systems. Also separation of interference when multiple of the sources combine is critical for making correct action to mitigate the problem caused by the corresponding problem, which is presented in Chapter 3[1].

Information bearing symbols are put along frequency dimension in multicarrier communication systems. Consequently, in OFDM as a multicarrier communication considered in this thesis, interference type that is analogous to inter-symbol interference (ISI) in single carrier systems is inter-carrier interference (ICI) in time varying channels. As ISI is investigated and visualized via eye patterns constructed by received time signals, interference between subcarriers of OFDM signal needs to be able to observed via a diagram in frequency domain. Thus as given in Chapter 4[2], a method to construct frequency domain eye diagrams for OFDM signals is developed. Finally, we conducted some other research along the thesis process [24] that is not included in this thesis.

1.1 Organization of Thesis

This thesis consists of five chapters. Chapter 2 introduces an overview of OFDM systems including basic elements with radio frequency (RF) and digital baseband signal processing aspects. Performance-limiting problems of OFDM are analyzed as well. In Chapter 3, a practical visualization and identification method including special frame design and the reception method for interferences in OFDM is given. Different sources of impairments that result in similar consequences are separated from each other with proposed method. Also, simulation and the measurement results of the proposed scheme are given. Chapter 4 introduces eye diagram in frequency domain for OFDM waveforms as another interference identification tool. With proposed method, time varying impairments such as frequency spreading and CFO that result in ICI are investigated and identified. Simulation and mea-

[1]This work is submitted to [22].
[2]This work is published in [23].

surement results are also given at the end of the chapter. Chapter 5 concludes the thesis with summary and discussion of open research areas.

CHAPTER 2:

AN OVERVIEW OF ORTHOGONAL FREQUENCY-DIVISION MULTIPLEXING

2.1 Introduction

In this chapter, main principles of orthogonal frequency-division multiplexing (OFDM) are introduced. Time and spectral characteristics of the waveform and use of guard period are explained. Then, main impairments associated with OFDM are analyzed and corresponding countermeasures are referred. Finally, a basic OFDM baseband communication system is given along with the building blocks with their functions.

2.2 System Model

OFDM signal can be interpreted as combination of multiple sinusoidal signals with different (and orthogonal to each other) frequencies. Each sinusoidal signal has an amplitude and phase that represents the information to be carried. In other words, each sinusoid, referred as subcarrier of OFDM symbol, is a phase-shift keying (PSK) or quadrature amplitude modulation (QAM) signal. Envelope of each subcarrier, i.e., pulse shape, is rectangular. Thus, continuous time representation of an OFDM symbol is given as

$$x_m(t) = \sum_{k=-N/2}^{N/2-1} X_{m,k} e^{j2\pi(f_c+k\Delta f)t}, \quad 0 \leq t < T_{\mathrm{U}}, \tag{2.1}$$

where $X_{m,k}$ is complex number representing the information symbol on kth subcarrier of mth OFDM symbol, N is the number of subcarriers, f_c is carrier frequency, and Δf is subcarrier spacing along frequency. Note that rectangular pulse shape with duration of T_{U} corresponds to sinc-shaped (i.e., $\frac{\sin(\pi T_{\mathrm{U}} f)}{\pi T_{\mathrm{U}} f}$) subcarrier shifted with $k\Delta f$ along frequency

domain. Therefore, as dual of the *Nyquist condition for zero ISI* [25] implies, selecting $1/\Delta f = T_{\mathrm{U}}$ satisfies the orthogonality between subcarriers, i.e., zero inter-carrier interference (ICI) condition.

Before transferring to discrete-time domain, we define discrete Fourier transform (DFT) which constitutes the core of the OFDM modulation/demodulation stages. DFT of a M-length sequence (time domain signal in given context) is defined as

$$F(l) = \sum_{m=0}^{N-1} f(m) e^{-j\frac{2\pi lm}{M}}, \tag{2.2}$$

and inverse of this operation, inverse discrete Fourier transform (IDFT), is given as

$$f(m) = \frac{1}{M} \sum_{l=0}^{N-1} F(l) e^{j\frac{2\pi lm}{M}}. \tag{2.3}$$

When we sample baseband OFDM symbol in (2.1) with sampling rate of $N\Delta f$, which is also the Nyquist rate of continuous signal, discrete time symbol becomes the folded version of IDFT of the complex symbol vector as

$$x_m(n) = \frac{1}{N} \sum_{k=0}^{N-1} X_{m,k} e^{j\frac{2\pi kn}{N}}, \quad 0 \leq n \leq N-1. \tag{2.4}$$

Therefore, each pure OFDM symbol is generated by IDFT of the information bearing data sequence.

2.2.1 Multipath Channel and Circular Convolution

The effect of multipath channel on signal is modeled as filtering the signal with a finite impulse response (FIR) filter, i.e., linear convolution of signal with the channel impulse response. When it comes to compensating the distortion effect of the channel, main advantage of OFDM emerges as iti is used with guard period. Considering discrete implementation, convolution of tho sequences corresponds to multiplication of their DFT's if the sequences are circularly convolved. Thus, in order to be able to perform frequency

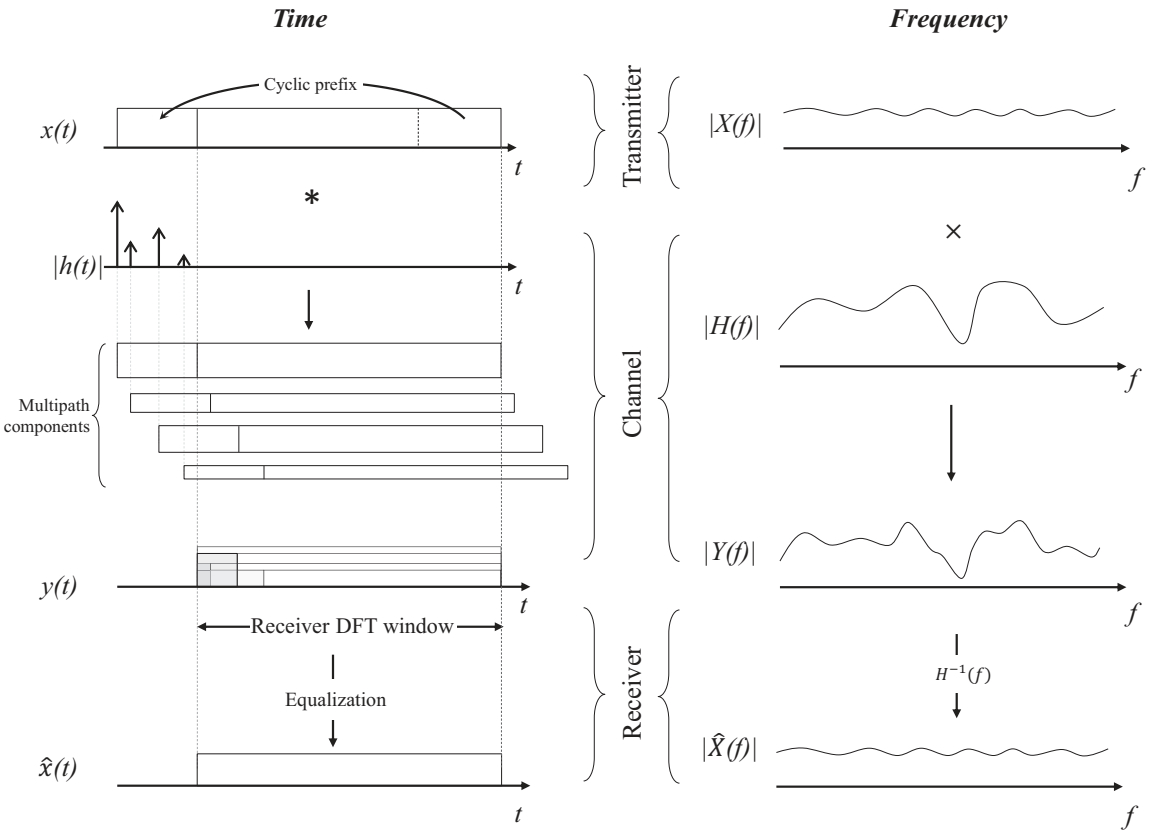

Figure 2.1 Time-frequency illustration of multipath channel and CP usage in OFDM.

domain equalization (FDE) by simply multiplying the DFT of received symbol with inverse of channel frequency response, filtering should be circular. This is achieved by concatenating a copy of the last of pure OFDM symbol to the beginning. After the cyclic insertion, cyclic prefix (CP), OFDM symbol can be redefined by extending the time index in (2.4) as $-N_{\mathrm{G}} \leq n \leq N$ where N_{G} is the guard size in samples. The length of CP needs to be at least as length of FIR to guarantee the circularity. Figure 2.1 shows the CP usage, wireless channel, and equalization in both time and frequency domain in OFDM systems.

2.2.1.1 Cyclic Prefix or Zero Padding?

Alternative to CP insertion at the transmitter, circularity can also be achieved at the receiver. For this, silent period is allocated before the symbol with same time constraint of CP, which is called as zero padding (ZP). In ZP, the circularity is achieved via an additional

process at the receiver: Adding the residual of the received symbol due to multipath spread to the beginning of the symbol before DFT. Both methods satisfy the zero-ICI criterion. However, CP is mostly chosen alternative as guard time for the reasons that are itemized below:

- Repeating feature of OFDM symbol with CP can be utilized for time/frequency synchronization, or enhancing the existing synchronization procedure.
- ZP method introduces more noise since the residual part that is added to the beginning of the symbol at the receiver also includes independent noise terms, which degrades the signal-to-noise ratio (SNR) of the signal to be demodulated.
- Transmit waveform modifications such as time domain windowing can be implemented along with CP, but not ZP.

Although ZP method is more power-efficient due to silent guard duration at the transmitter side and cyclic features of the CP-OFDM increase the detection probability in secure-communications, aforementioned facts were found sufficient for CP to be adopted by most of the applications.

2.3 OFDM Impairments

OFDM signal gets distortion by various impairments in various stages of the communication link. The reason for the problem might be the time-spreading, or time variance in the wireless multipath channel, timing and carrier frequency disagreement between the transmitter and receiver as an hardware-based problem, or problems that emerges with the characteristics of the OFDM waveform such as high peak-to-average power ratio (PAPR) and out-of-band emission.

In addition, noise, which exists as a combination of thermal background noise, electrical noise in the receiver components such as amplifiers, mixers, and filters, degrades the received signal quality. The noise in communication systems is modeled as additive white

Gaussian noise (AWGN) since it additively distorts the signal, its samples are independent and identically distributed (i.i.d.) that makes it white, and Gaussian distributed.

2.3.1 Channel Impairments

2.3.1.1 Insufficient Guard Time

Wireless channel spreads the transmitted signal in time since the radio waves travel through multiple paths that have different propagation delays, amplitudes and phases. Without considering the noise, received signal for mth symbol can be written as

$$y_m(n) = \sum_{\ell=0}^{L-1} h(\ell, n) \sum_{i=-1}^{0} x_{m+i}(n - i(N + N_{\mathrm{G}}) - \ell), \quad 0 \leq n \leq N-1 \tag{2.5}$$

where $h(\ell, n)$ is impulse response of the channel at time n. For this part assume there is no time variation in the channel, $h(\ell, n) = h(\ell)$. By interchanging the summations in (2.5), received symbol can be then rewritten as

$$y_m(n) = \sum_{\ell=0}^{n+N_{\mathrm{G}}} h(\ell) x_m(n-\ell) + \sum_{\ell=n+N_{\mathrm{G}}+1}^{L-1} h(\ell) x_{m-1}(n + (N + N_{\mathrm{G}}) - \ell) \tag{2.6}$$

$$= \underbrace{\sum_{\ell=0}^{L-1} h(\ell) x_m(n-\ell)}_{\text{Desired signal}} - \underbrace{\sum_{\ell=n+N_{\mathrm{G}}+1}^{L-1} h(\ell) x_m(n-\ell)}_{\text{Interference due to loss of orthogonality}}$$

$$+ \underbrace{\sum_{\ell=n+N_{\mathrm{G}}+1}^{L-1} h(\ell) x_{m-1}(n + (N + N_{\mathrm{G}}) - \ell)}_{\text{Inter-symbol interference}} \tag{2.7}$$

It is clear from (2.7) that when $N_{\mathrm{G}} \geq L - 1$, i.e., guard time against multipath distortion is sufficient, the second and the third terms disappear which are interference due to loss of orthogonality between subcarriers and inter-symbol interference (ISI) respectively. Detailed analysis will be provided in the next chapter including the receiver chain.

2.3.1.2 Time Variation

Mobility of the transmitter or receiver antennas, or temporal changes in the wireless propagation environment makes the channel time varying. Analogous to frequency selectivity of time spreading channels, time selective channels results in spreading in frequency. Although OFDM is designed to cope with time spreading with guard period, it has no countermeasure for frequency spreading. In other words, any channel variation in the symbol duration results in some ICI because sinc-subcarriers are strictly overlapped and have high sidelobes. When we take the DFT of the received signal in (2.5) in time varying case by assuming sufficient CP size, frequency domain symbols can be obtained as

$$
\begin{aligned}
Y_{m,q} =& \frac{1}{N}\sum_{n=0}^{N-1} y_m(n) e^{-j\frac{2\pi qn}{N}} && (2.8)\\
=& \frac{1}{N}\sum_{n=0}^{N-1}\left(\sum_{\ell=0}^{L-1} h(\ell,n)x_m(n-\ell)\right)e^{-j\frac{2\pi qn}{N}} && (2.9)\\
=& \frac{1}{N}\sum_{n=0}^{N-1}\left(\sum_{\ell=0}^{L-1} h(\ell,n)\Big(\sum_{k=0}^{N-1} X_{m,k}e^{j\frac{2\pi k(n-\ell)}{N}}\Big)\right)e^{-j\frac{2\pi qn}{N}} && (2.10)\\
=& \sum_{k=0}^{N-1} X_{m,k}\left(\sum_{\ell=0}^{L-1}\Big(\frac{1}{N}\sum_{n=0}^{N-1} h(\ell,n)e^{j\frac{2\pi(k-q)n}{N}}\Big)\right)e^{-j\frac{2\pi k\ell}{N}} && (2.11)\\
=& X_{m,q}\frac{1}{N}\sum_{n=0}^{N-1}\underbrace{\left(\sum_{\ell=0}^{L-1} h(\ell,n)e^{-j\frac{2\pi q\ell}{N}}\right)}_{H_q(n)} \\
&+ \sum_{\substack{k=0,\\ k\neq q}}^{N-1} X_{m,k}\underbrace{\left(\sum_{\ell=0}^{L-1}\Big(\frac{1}{N}\sum_{n=0}^{N-1} h(\ell,n)e^{j\frac{2\pi(k-q)n}{N}}\Big)\right)e^{-j\frac{2\pi k\ell}{N}}}_{H_{q,k}}. && (2.12)
\end{aligned}
$$

Note that in (2.5) the first term is the desired signal multiplied by the time-average of the channel frequency responses (CFR) for $n = \{0, ..., N-1\}$ and the second term is the ICI from kth subcarrier to qth subcarrier including the channel effect. In general, received symbol in frequency can be written in terms of matrix form as

$$\mathbf{y} = \mathbf{H}\mathbf{x} \tag{2.13}$$

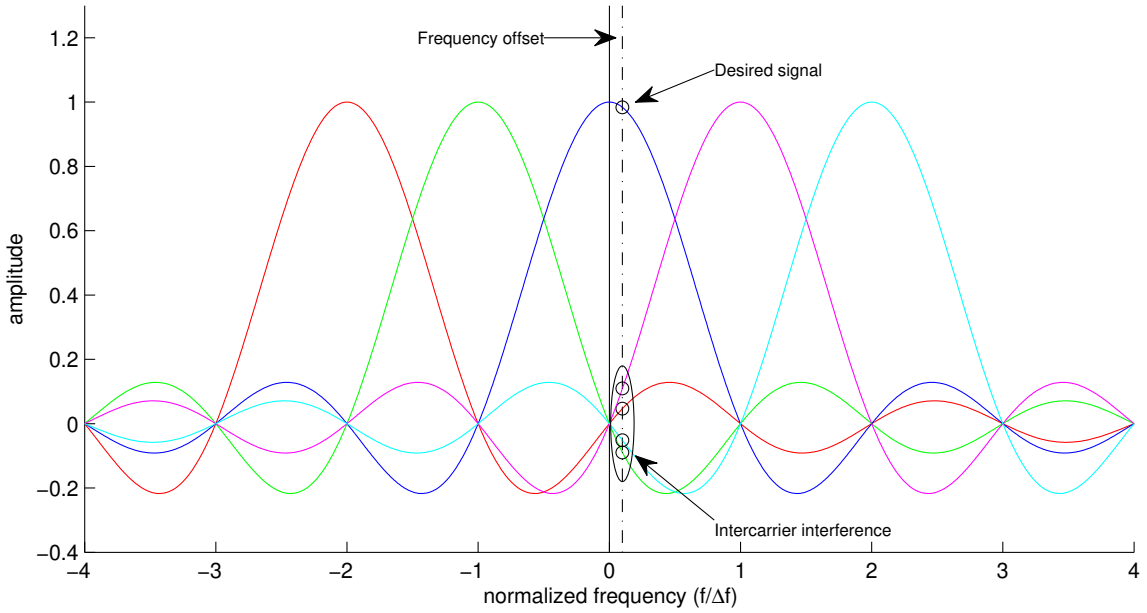

Figure 2.2 Inter-carrier interference in the presence of carrier frequency offset.

where **y** is column vector of received frequency domain symbols, **H** is channel matrix with diagonal terms, $H_{q,q} = H_q(n)$, are CFR at each subcarrier location and remaining terms, $H_{q,k}$, are ICI gains with channel effect.

Although main channel-related interferences caused by insufficient CP and time variation are given separately, their analysis and identification when both exist at the same time will be given in the following chapter.

2.3.2 Hardware-Based Impairments

2.3.2.1 Frequency Offset

Local oscillators that are used to upconvert the baseband signal to radio frequency (RF) at the transmitter and to downconvert the RF signal to baseband cannot run synchronously due to physical separation of the wireless nodes. Carrier frequency offset (CFO), which occurs due to misalignment between carrier frequencies, ruins the orthogonality between subcarriers. Since it shifts the signal in frequency domain where the subcarriers are strictly orthogonal as illustrated in Figure 2.2, CFO is a critical problem in OFDM if not compensated. In literature, CFO is generally represented as the ratio of offset to the sub-

carrier spacing. By assuming normalized frequency offset is $\epsilon = f_{\text{offset}}/\Delta f$, received OFDM symbol without any other impairment can be written as

$$y_m(n) = x_m(n)e^{j(\frac{2\pi\epsilon n}{N}+\phi)}, \quad 0 \le n \le N-1 \tag{2.14}$$

where ϕ is phase offset betweeen the local oscillators. By the DFT of $y_m(n)$ and omitting the symbol index, frequency domain symbol becomes

$$Y_q = \sum_{n=0}^{N-1} \Big(x(n)e^{j(\frac{2\pi\epsilon n}{N}+\phi)}\Big)e^{-j\frac{2\pi qn}{N}} \tag{2.15}$$

$$= e^{j\phi}\sum_{n=0}^{N-1}\left(\Big(\frac{1}{N}\sum_{k=0}^{N-1}X_{m,k}e^{j\frac{2\pi kn}{N}}\Big)e^{j\frac{2\pi\epsilon n}{N}}\right)e^{-j\frac{2\pi qn}{N}} \tag{2.16}$$

$$= \frac{e^{j\phi}}{N}\sum_{k=0}^{N-1}X_{m,k}\sum_{n=0}^{N-1}e^{j\frac{2\pi(k-q+\epsilon)n}{N}} \tag{2.17}$$

By using geometric series expansion for the inner summation in (2.17), received symbol can be clearly represented as

$$Y_q = \frac{e^{j\phi}}{N}\sum_{k=0}^{N-1}X_k\frac{1-e^{j2\pi(k-q+\epsilon)}}{1-e^{j2\frac{\pi}{N}(k-q+\epsilon)}} \tag{2.18}$$

$$= \frac{e^{j\phi}}{N}\sum_{k=0}^{N-1}X_k\frac{e^{-j\pi(k-q+\epsilon)}-e^{j\pi(k-q+\epsilon)}}{e^{-j\frac{\pi}{N}(k-q+\epsilon)}-e^{j\frac{\pi}{N}(k-q+\epsilon)}}\frac{e^{j\pi(k-q+\epsilon)}}{e^{j\frac{\pi}{N}(k-q+\epsilon)}}\frac{-1/2j}{-1/2j} \tag{2.19}$$

$$= \frac{e^{j\phi}}{N}\sum_{k=0}^{N-1}X_k\frac{\sin\big(\pi(k-q+\epsilon)\big)}{\sin\big(\frac{\pi}{N}(k-q+\epsilon)\big)}e^{j\pi(1-\frac{1}{N})(k-q+\epsilon)}. \tag{2.20}$$

Therefore, similar to time variation case, received symbol can be written as

$$Y_q = \underbrace{X_q\frac{\sin\big(\pi\epsilon\big)}{N\sin\big(\frac{\pi}{N}\epsilon\big)}e^{j(\pi(1-\frac{1}{N})\epsilon+\phi)}}_{\substack{\text{Desired signal with attenuation}\\ \text{and phase rotation}}} + \underbrace{\sum_{\substack{k=0,\\ k\neq q}}^{N-1}X_k\frac{\sin\big(\pi(k-q+\epsilon)\big)}{N\sin\big(\frac{\pi}{N}(k-q+\epsilon)\big)}e^{j\left(\pi(1-\frac{1}{N})(k-q+\epsilon)+\phi\right)}}_{\text{ICI term}}. \tag{2.21}$$

In (2.21), the first term is attenuated and phase rotated desired subcarrier symbol as a function of normalized CFO. Phase term also includes the phase offset between local oscillators that can be compansated by channel estimation and equalization process. However, the attenuation of the desired symbol and the second term, ICI, degrades the signal quality, hence bit error rate (BER), if CFO is not compansated. There are several methods for estimating and compensating the CFO before DFT stage including utilizing pilot symbols, exploiting the repeating pattern of CP [26], and using the training sequence that consists of repeating subsequences [27, 28].

2.3.2.2 Receiver Timing Offset

Sampling timing offset can be considered as a part of the multipath channel and inherently compansated by the channal estimation and equalization if the total of timing offset and the chanel length does not exceed the guard duration of the symbol. Assume that sample time offset normalized to sampling duration T_{U}/N is θ. Then, received signal is given as

$$y_m(n) = x_m(n-\theta) \tag{2.22}$$

$$= \frac{1}{N}\sum_{k=0}^{N-1} X_{m,k} e^{j\frac{2\pi k(n-\theta)}{N}}, \quad 0 \le n \le N-1. \tag{2.23}$$

By performing DFT of the received symbol, we obtain

$$Y_{m,q} = \sum_{n=0}^{N-1}\left(\frac{1}{N}\sum_{k=0}^{N-1} X_{m,k} e^{j\frac{2\pi k(n-\theta)}{N}}\right) e^{-j\frac{2\pi qn}{N}} \tag{2.24}$$

$$= \frac{1}{N}\sum_{k=0}^{N-1} X_{m,k} e^{-j\frac{2\pi k\theta}{N}} \sum_{n=0}^{N-1} e^{j\frac{2\pi(k-q)n}{N}} \tag{2.25}$$

$$= X_{m,q} e^{-j\frac{2\pi q\theta}{N}}. \tag{2.26}$$

As can be seen from (2.26), effect of timing misalignment on the subcarrier symbol is solely phase rotation along frequency domain. Hence it can easily be considered multipath

channel effect and be compensated alongside the frequency selectivity. Along with the CFO, estimation of sample timing in OFDM is also studied in [26, 28].

In fact, CFO and timing offset are the duals of each other in frequency and time domains. However, time offset does not introduce impairment as long as guard time is sufficient while CFO degrades the performance since there is no guard in frequency domain, making the action for CFO a must.

2.3.3 Waveform-Based Impairments

Along with the channel- and hardware-based problems, specific characteristics of the OFDM waveform emerges such problems as high PAPR and out-of-band emission.

2.3.3.1 Peak-to-Average Power Ratio

PAPR is a general concern in waveforms that consist of multiple independent information symbols in time such as code division multiple access (CDMA) and multicarrier schemes in general. In OFDM, high number of subcarriers increases the probability of getting high instantaneous power because independent subcarriers might combine constructively for some time samples. PAPR of discrete time OFDM symbol with N subcarriers can be written as

$$PAPR_m = \frac{\max_{0\leq n\leq N-1} |x_m(n)|^2}{\mathrm{E}[|x_m(n)|^2]} \tag{2.27}$$

where $\mathrm{E}[\cdot]$ is expected value operation. By assuming worst case scenario where all PSK-modulated subcarrier symbols constructively added at a specific sample, $PAPR$ becomes

$$\begin{aligned} PAPR_{\text{worst}} &= \frac{|NA|^2}{NA^2} \\ &= N. \end{aligned} \tag{2.28}$$

where A is the maximum magnitude of the complex subcarrier symbol. PAPR increases as the number of subcarriers increases. When we consider the high number of subcarriers,

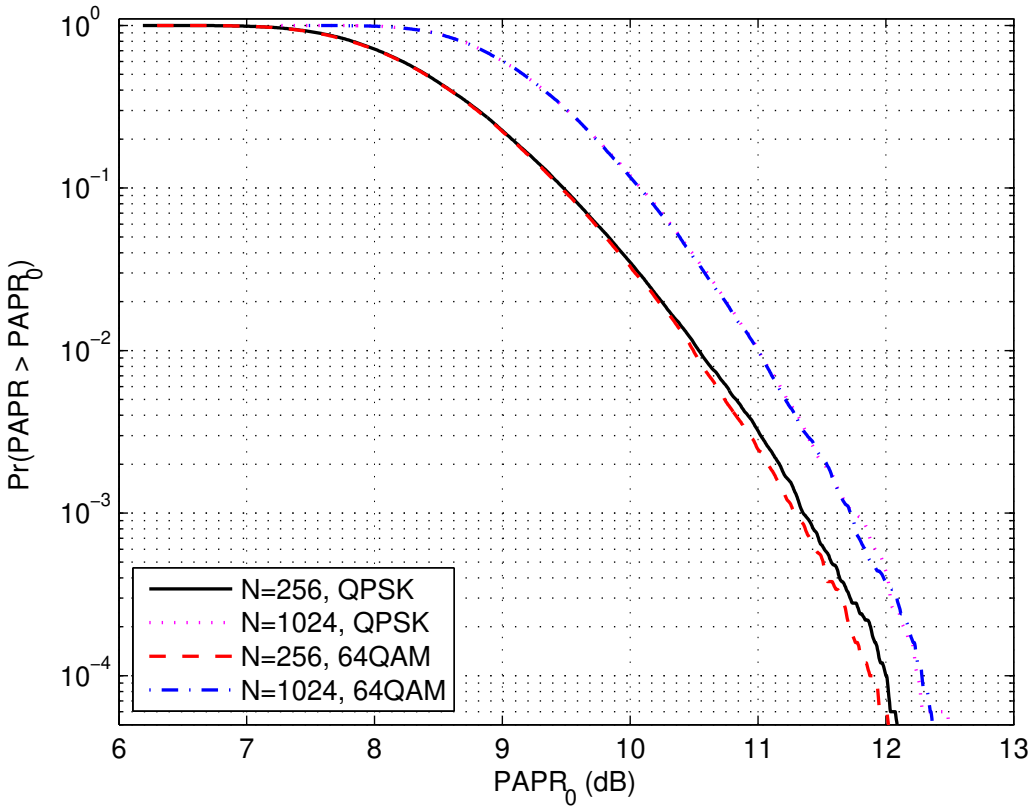

Figure 2.3 CCDF of PAPR for OFDM signal for N=256 and 1024 with QPSK and 64QAM.

central limit theorem applies that the signal in time becomes zero-mean complex-valued near Gaussian distributed random variables, independent of the modulation type used. The impact of subcarrier numbers as well as the modulation type can be observed from Figure 2.3 in which complementary cumulative distribution functions (CCDF) of PAPR for OFDM signal with $N = 256$, $N = 1024$ along with quadrature phase-shift keying (QPSK) and 64QAM modulations are given.

PAPR of signal becomes critical when it is fed to power amplifier at transmitter. Signals with high peak power pushes the operating point of the power amplifier to nonlinear region of power amplifier, which results in distortion in amplified signal. In other words, amplitde and phase distortion of power amplifier introduces spectral regrowth distorting the other users in the adjacent band, and in-band distortion degrading the BER. When time domain windowing is performed for sidelobe suppression, nonlinearity of power amplifier

becomes dominant and spectral regrowth effect can be observed. In Figure 2.5 power spectrums with several input back-offs (IBO), which is the ratio between 1 dB compression point input-referred power and the input signal average power [29], are given. Saleh's widely-adopted model [30] is used for power amplifier implementation. We neglect the effect of PAPR on the OFDM in this thesis.

In order to reduce PAPR of the OFDM signal, various methods are proposed including amplitude clipping, coding, partial transmit sequence, selected mapping, interleaving, and tone reservation for details of which [31] can be referred.

2.3.3.2 Spectral Sidelobes

OFDM signal has high spectral sidelobes due to rectangular transmit pulse. Out-of-band emission creates interference to other users, called adjacent channel interference (ACI). Especially with the emerge of cognitive radio (CR) applications whose strongest candidate is OFDM, spectral containment is a critical concern. There are various countermeasures to spectral sidelobes that can be considered under two main categories as data independent methods, which are relatively simpler to implement, and data-dependent methods, which takes the data symbols into account for spectral sidelobe suppression.

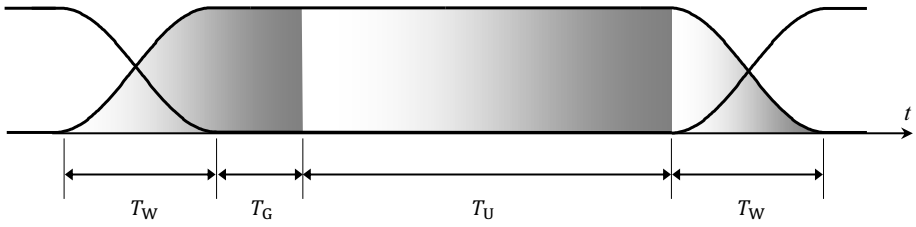

Figure 2.4 Time domain windowing for smoothing the symbol transitions.

The former category includes time domain windowing in which symbol transitions are smoothed by shaping the symbol extensions with specific function (illustrated in Figure 2.4), frequency domain guard subcarrier insertion edge-band subcarriers are nulled to let signal spectrum fall under some spectral mask. Other data-dependent techniques to suppress the sidelobes are dedicating the edge subcarriers for sidelobe cancellation according to

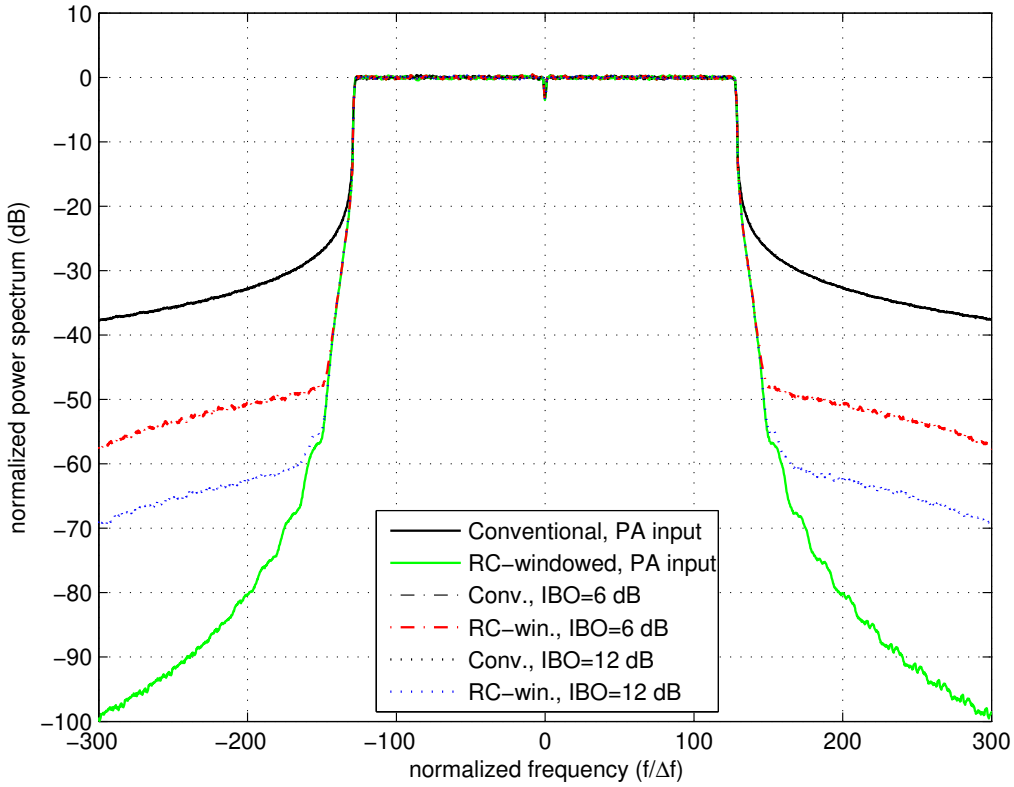

Figure 2.5 Power spectrum for windowed and conventional OFDM signal before and after the power amplifier with different input back-offs.

data combination [32], weighting the subcarriers to suppress the sidelobes [33], mapping the original data sequence to multiple and selecting the one that has least sidelobe power [34], designing the symbol transition periods adaptively depending on the data symbols [35], precoding to make emitted signals phase and amplitude continuous [36], and orthogonal projection of the transmitted symbols to provide deeper suppression out of the band [37]. On the first hand, data dependent techniques give good suppression results but they are computationally complex due to symbol-by-symbol processing requirement. Also, [32] increases the PAPR, [33] and [36] degrade the bit error rate performance, and [34] and [37] require additional information from the transmitter for symbol recovery. On the other, time domain windowing technique is simpler and computationally efficient alternative to reduce

out-of-band emission [38] with the penalty of redeuced spectral efficieny due to symbol extension in time.

Raised-cosine (RC) function is widely adopted for filtering the rectangular OFDM pulse. Figure 2.5 shows the spectrum of the OFDM signal with and without RC windowing for $N = 256$, $N_{\mathrm{G}} = 16$, and $N_{\mathrm{W}} = 16$. Also, the effect of power amplifier can be observed. By considering the use of practical amplifier, any of the aforementioned spectral suppression techniques need to be reconsidered since the regrowth in the sidelobes after power amplifier makes the afford for suppression ineffective.

CHAPTER 3:

INTERFERENCE VISUALIZATION AND IDENTIFICATION FOR OFDM-BASED SYSTEMS

3.1 Introduction

Orthogonal frequency-division multiplexing (OFDM) has been widely adopted because of its robustness against multipath channel, flexibility, and efficiency. However, OFDM suffers from various types of interferences caused by doubly dispersive channel and RF front end impairments. In the conventional testing and measurement of communication systems, total interference is considered rather than identifying the source of impairments separately. Evaluation based on total effective interference can give misleading information about the system and the impairment that is present. On the other hand, interference identification and separation give insight into the source of the problem, helping to combat interference.

In OFDM, different impairments in the system may result in similar consequences at the receiver end. For example, overlapping subcarriers that have high sidelobes due to rectangular pulse shape makes OFDM very sensitive to inter-carrier interference (ICI) in the presence of time varying impairments such as frequency spread, carrier frequency offset (CFO), and phase noise. Since there is only one frequency at which the reception introduces no contribution from neighboring subcarriers, any impairment that spreads (or shifts) the signal in frequency destroys the orthogonality between the subcarriers. Besides, any insufficient guard interval ruins the orthogonality leading to ICI from the subcarriers of the current symbol, and also inter-symbol interference (ISI) from the previous symbol, resulting in interference on the subcarriers of the current symbol. In addition to ICI and ISI, other user's interferences such as narrow band interference (NBI) and adjacent channel

interference (ACI) are substantial elements because OFDM is one of the strongest candidates for networks adopting opportunistic spectrum usage. For instance, unlicensed users that utilize OFDM suffer from NBI in the presence of licensed user signal in its transmission band. Also, effect of ACI on the OFDM system performance is no less than that of other communication schemes especially with the high out-of-band emission of OFDM signal.

Interference mitigation, cancellation and avoidance techniques for OFDM are quite well studied in the literature (e.g. see [39] and references therein). In [40], the effects of time selective multipath fading are investigated for OFDM. Also, performance analysis and optimization for OFDM systems in doubly dispersive channels are performed while characterization of ISI and ICI are considered separately in [41, 42]. However, awareness, identification, and separation of different interference sources in OFDM systems needs more afford in the literature for the sake of developing interference immune systems, as well as for better testing and measurement of the OFDM based systems.

Therefore, main focus of this chapter is to introduce visualization and identification of

1. ISI and ICI due to the insufficient cyclic prefix (CP),
2. ICI due to the time varying channel,
3. NBI and ACI due to the other users or systems

in OFDM-based communication systems by transmitting special set of waveforms. Interference is visualized by spectrogram-like diagram, referred as interference spectrogram, and analysis of the received signal is performed for identification of interference sources and separation of interferences when multiples are existing at hte same time. Proposed interference visualization and identification techniques yield better understanding of the interference sources in OFDM-based systems. Instead of the average or combination of different interferences, it is possible to visually observe and separate the self-interferences like ICI and ISI from each other. Other user's interferences like NBI and ACI are also clearly observed with proposed method.

Remaining of this chapter is organized as follows: In Section 3.2, the system model is introduced. Then, interference spectrogram and the identification are demonstrated including examples for various cases in Section 3.3. The performance analysis based on simulations and measurements is given in Section 3.4. Finally, conclusions are drawn in Section 3.5.

3.2 System Model

We consider an OFDM system in which transmitter generates symbols by processing complex baseband symbol vector $\mathbf{X} = [X(0), X(1), ..., X(N-1)]^T$ with inverse discrete Fourier transform (IDFT) operation. After insertion of cyclic prefix (CP), OFDM symbol is converted to time-domain signal before being transmitted through the wireless channel. The time-domain complex envelope of the baseband signal at the transmitter can be written as

$$x(t) = \sum_{m=-\infty}^{+\infty} \sum_{k=0}^{N-1} X_m(k) e^{j2\pi\Delta f(t-T_{\mathrm{G}}-mT_{\mathrm{S}})} \tag{3.1}$$

where m is the OFDM symbol index, T_{G} and $T_{\mathrm{S}} = T_{\mathrm{U}} + T_{\mathrm{G}}$ are the CP and total symbol durations, T_{U} is useful symbol duration, $\Delta f = 1/T_{\mathrm{U}}$ is the subcarrier spacing, and $X_m(k)$ is the complex information bearing symbol corresponding to kth subcarrier of mth OFDM symbol.

The transmitted OFDM signal is affected by a time varying multipath channel. The channel between the transmitter and the receiver is modeled as

$$h(\tau, t) = \sum_{\ell=0}^{L-1} \alpha_\ell(t)\delta(\tau - \tau_\ell) \tag{3.2}$$

where L is the total number of multipath components, α_ℓ is the complex gain and τ_ℓ is the delay of the ℓth component. Then, the received signal is written as

$$y(t) = \sum_{\ell=0}^{L-1} \alpha_\ell(t)x(t - \tau_\ell) + w(t) \tag{3.3}$$

where $w(t)$ is the additive white Gaussian noise (AWGN).

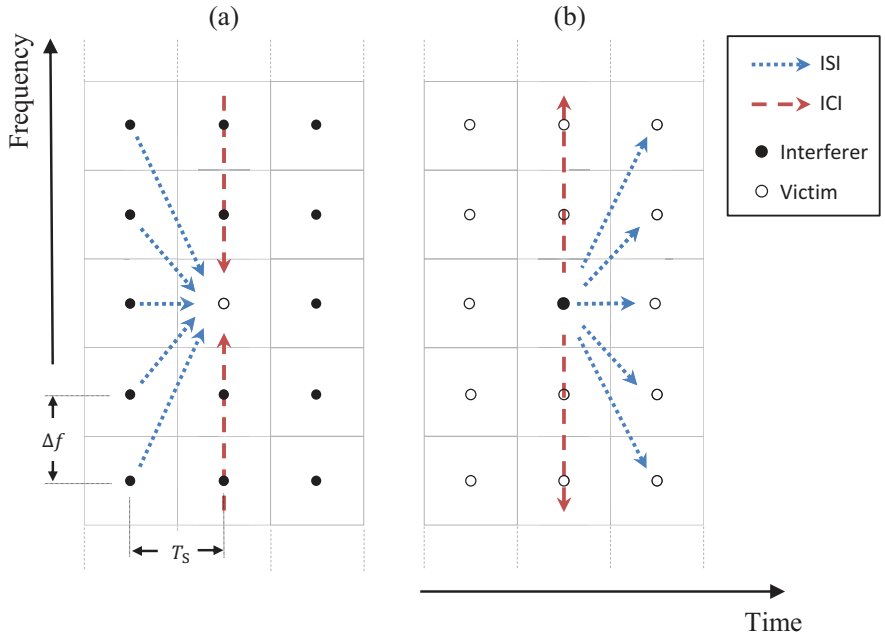

Figure 3.1 Time-frequency lattice representation of OFDM with two approaches to ISI and ICI. (a) Multiple interferers with one victim and (b) one interferer with multiple victims.

3.3 Interference Spectrogram

Interferences in OFDM systems can be considered under two main categories as other-signal interference and self-interference. While NBI and ACI are the interferences originated by other sources, i.e., unintended transmitters, ISI and ICI fall under the self-interference since the source of problem is the same signal itself. We consider a spectrogram-like diagram in which all the aforementioned interferences can be visualized. Two different modes for interference spectrogram are introduced. In the first mode, which can also be considered as introductory mode, other-signal interferences are mainly investigated as well as self-interferences. Then second mode of interference spectrogram is given for self-interference identification and separation.

In conventional approach, interference is considered as the contribution from all other subcarriers in a specific victim subcarrier as in Figure 3.1(a). Since the victim sub-

carrier is left empty at the transmitter, observed signal power corresponds to the interference from other symbols and subcarriers due to the loss of orthogonality. However, we adopt another approach to be able to investigate different interferences in a single diagram. For this purpose, a set of OFDM symbols, in which one subcarrier is activated for each symbol, is generated at the transmitter side. For interference spectrogram concept introduced in this study, it is critical to realize that transmitting one active subcarrier solely for each OFDM symbol corresponds to considering one interferer (active) subcarrier and multiple victim (passive) subcarriers as indicated in Figure 3.1(b). Since the total interference on one subcarrier from the other subcarriers is equal to the total interference caused by one subcarrier to other subcarriers, interference analysis and results do not alter, whose proof will be given in Section 3.3.1.

3.3.1 Spectrogram Mode 1

In the first mode of interference spectrogram, frame is structured as the subcarriers are activated in a sweeping manner with increasing index for consecutive symbols and remaining subcarriers are zeroed as illustrated in Figure 3.2(a). Sampled time-domain representation of complex envelope of OFDM symbols in the frame are then given by

$$x_m(n) = \sum_{k=0}^{N-1} X_m(k) e^{j\frac{2\pi}{N}kn}, \qquad m = 0, \ldots, N-1,$$
$$n = -N_{\mathrm{G}}, \ldots, N-1, \tag{3.4}$$

where N_{G} is CP size, m is symbol index, and activation of the subcarriers in the frame are configured as

$$X_m(k) = \begin{cases} 1, & \text{for } k = m + N/2, \quad 0 \le m \le N/2 - 1, \\ 1, & \text{for } k = m - N/2, \quad N/2 \le m \le N - 1, \\ 0, & \text{otherwise.} \end{cases} \tag{3.5}$$

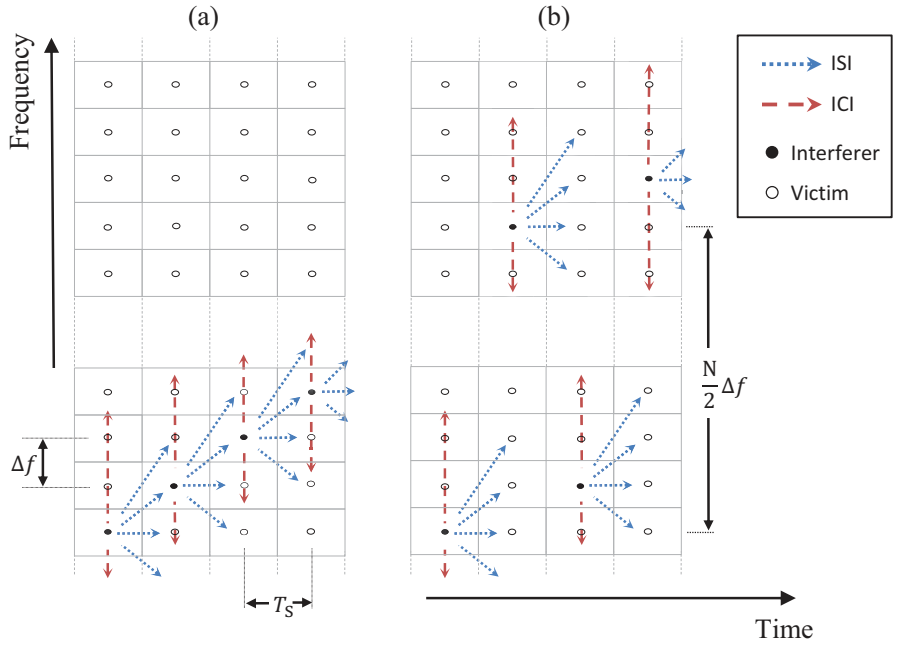

Figure 3.2 Construction of frame structure for interference spectrogram. (a) First mode of subcarrier activation with increasing order and (b) second mode of subcarrier activation with hopping order.

Subcarrier activation is started from $N/2$ so that sweeping starts from the leftmost subcarrier and ends at the rightmost subcarrier in the system band. Sending one subcarrier for each OFDM symbol provides clear sight of the impairment on the nulled subcarriers. After discrete Fourier transform (DFT) at the receiver side, power vector of each received symbol is put along the x axis and the vectors for consecutive symbols are put along y axis. Thus, the resulting plot gives a spectrogram-like diagram as in Figure 3.3(a). ICI is clearly observed as two bands surrounding active subcarriers along anti-diagonal of spectrogram. The presence of other user's signal in-band and adjacent band is revealed by two dimensional interference plot as narrow-band and adjacent channel interferences, respectively. Figure 3.3(b) shows simulated interference spectrogram with a NBI at 40th subcarrier of the received OFDM signal, as well as leaking power from lower adjacent channel. Note that the ACI originated from the lower frequency band also has an image at the right-

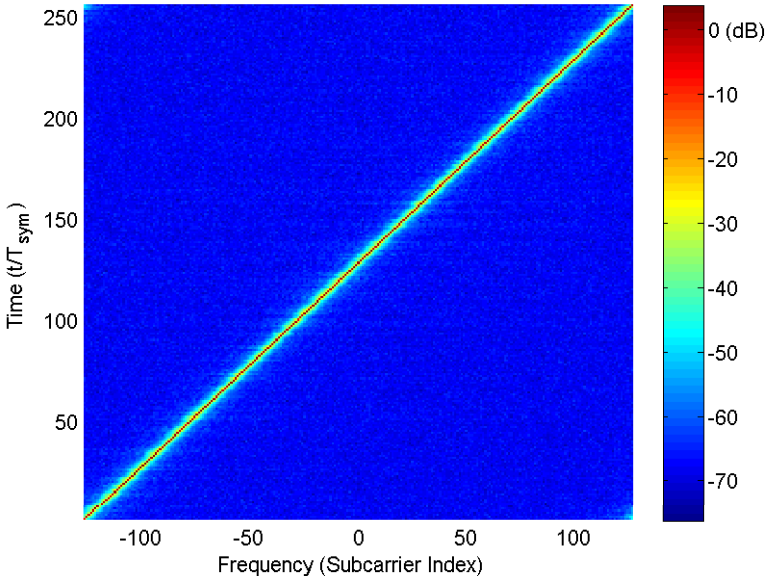

(a)

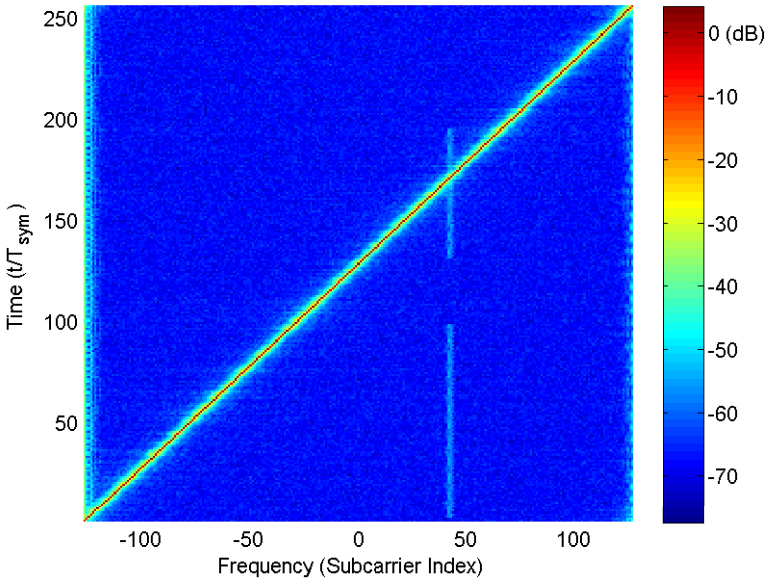

(b)

Figure 3.3 Interference spectrograms with increasing subcarrier index in (a) absence and (b) presence of NBI along with NBI.

most subcarriers because of the circularness of the DFT operation performed at the OFDM receivers.

CP insertion gives robustness against delay spread and timing errors by providing circular convolution of channel and signal. If the size of CP does not suffice the maximum

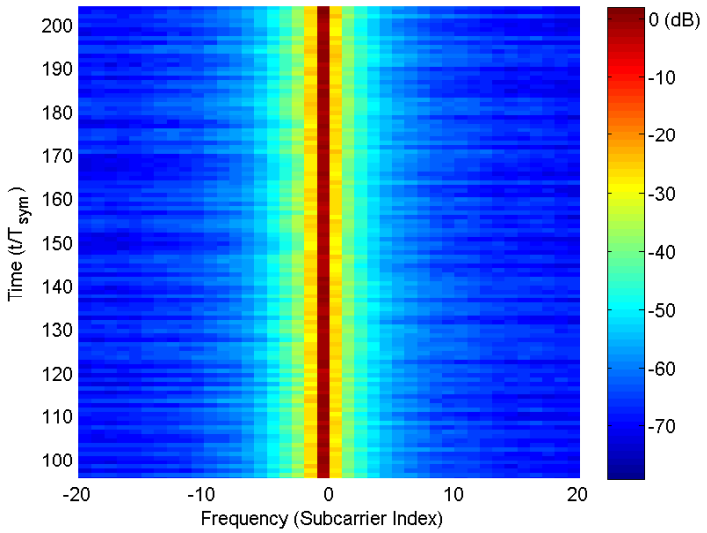

Figure 3.4 Aligned interference spectrogram when both ISI and ICI present.

excess delay and timing offset, ISI due to the leakage from the same subcarrier ($I_{\mathrm{ISI,SC}}$) and other subcarriers ($I_{\mathrm{ISI,OC}}$) of previous symbol occur. In addition, insufficient CP causes ICI between subcarriers of the current symbol, which is referred as $I_{\mathrm{ICI,LO}}$, because of the loss of orthogonality between subcarriers. It is worthed to note that although it leaks from other subcarriers, $I_{\mathrm{ISI,OC}}$ is considered as ISI since interference caused by the subcarriers of the previous OFDM symbol. Independent from the CP size, time selective channels result in ICI regardless of consecutive symbols. Interference that is originated from time varying channel impairments is referred as $I_{\mathrm{ICI,TS}}$.

3.3.2 Spectrogram Mode 2

Other-signal interferences are observed with spectrogram-like nature of the diagram in the first mode of subcarrier activation. However, when maximum excess delay of the channel is longer than the CP size, mth symbol whose $(m + N/2)$th subcarrier is activated gets leakage from $(m - 1)$th symbol in which $(m + N/2 - 1)$th subcarrier is active. Consequently, $I_{\mathrm{ISI,OC}}$ and $I_{\mathrm{ICI,LO}}$ are combined near the active subcarriers, making the identification of one from other a difficult task. This can be observed from Figure 3.4 where activated subcarriers are aligned to be observed as a straight line. Interference cloud at

the left part of active subcarrier line is slightly thicker than that at the right. By taking into account that time index increases along y axis, thicker cloud indicates that exist ISI from previous symbols on top of ICI. Therefore, to be able to distinguish $I_{\mathrm{ISI,SC}} + I_{\mathrm{ISI,OC}}$ from $I_{\mathrm{ICI,LO}}$, activated subcarrier of current symbol is located to the circularly farthest possible index from that of previous symbol in the second mode of interference spectrogram. Subcarrier mapping along OFDM symbols in the frame is then reconfigured as

$$X_m(k) = \begin{cases} 1, & \text{for } k = (m+N)/2, \quad m : \text{even}, \\ 1, & \text{for } k = (m-1)/2, \quad m : \text{odd}, \\ 0, & \text{otherwise}, \end{cases} \tag{3.6}$$

so that the distance between the active subcarriers of consecutive symbols becomes $N/2$, which was one in the first mode (3.5). Hopping subcarrier activation is illustrated in Figure 3.2(b).

At the receiver side, interference spectrogram with hopping subcarrier order is generated by circularly shifting each OFDM symbol after DFT in order that active subcarriers are aligned as a straight line along time axis. Figure 3.5(a) and (b) show the resultant plots with CP size of $N/4$ (longer than the maximum excess delay) and $N/128$ (shorter than the maximum excess delay), respectively. While there is no observable interference in long CP case, interference contribution from previous symbols appears at subcarriers distances of $N/2$ when $T_{\mathrm{G}} < \tau_{L-1}$. Two components of interference in the case of short CP: $I_{\mathrm{ISI,OC}}$ with $I_{\mathrm{ISI,SC}}$ and $I_{\mathrm{ICI,LO}}$ emerge at the left and right halves of the interference plot, respectively. Profiles of two resultant interference components, i.e., expected interference power along frequency axis are identical as in Figure 3.5(c). To confirm the equality of two interference components and the result of proposed method, consider a simplified noiseless two-tap time varying channel. For the sake of tractability, time variation is modeled as CFO in the channel whose sampled-time domain response is given as

$$h(n) = \big(\alpha_0 \delta(n) + \alpha_1 \delta(n-D)\big) e^{j\frac{2\pi}{N}\epsilon n} \tag{3.7}$$

where α_0 and α_1 are independent complex channel tap gains, $D > N_{\mathrm{G}}$ is the delay of the second tap, and ϵ is normalized frequency offset with respect to Δf. By assuming perfect time synchronization, mth received symbol in the DFT window, which is the convolution of the transmitted signal and the channel, can be written as

$$y_m(n) = \alpha_0 x_m(n) e^{j\frac{2\pi}{N}\epsilon n} + \begin{cases} \alpha_1 x_{m-1}(n+N+N_{\mathrm{G}}-D) e^{j\frac{2\pi}{N}\epsilon n}, & 0 \le n \le D-N-1, \\ \alpha_1 x_m(n-D) e^{j\frac{2\pi}{N}\epsilon n}, & D-N_{\mathrm{G}} \le n \le N-1. \end{cases} \tag{3.8}$$

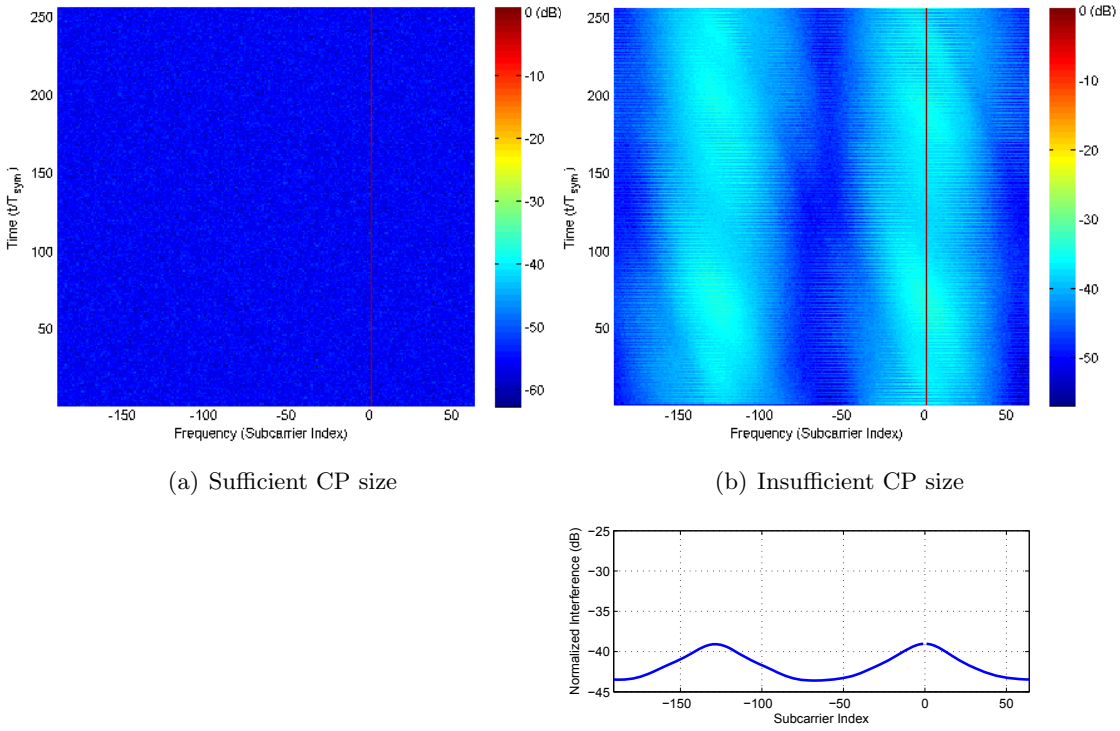

(a) Sufficient CP size

(b) Insufficient CP size

(c) Averaged spectrogram over time axis for (b).

Figure 3.5 Interference spectrograms for different CP sizes.

After the DFT operation, received signal on the lth subcarrier becomes

$$\begin{aligned} Y_m(l) =& \frac{1}{N}\sum_{n=0}^{N-1} \alpha_0 x_m(n) e^{j\frac{2\pi}{N}\epsilon n} e^{-j\frac{2\pi}{N}ln} \\ &+ \frac{1}{N}\sum_{n=0}^{D-N_{\mathrm{G}}-1} \alpha_1 x_{m-1}(n+N+N_{\mathrm{G}}-D) e^{j\frac{2\pi}{N}\epsilon n} e^{-j\frac{2\pi}{N}ln} \\ &+ \frac{1}{N}\sum_{n=D-N_{\mathrm{G}}}^{N-1} \alpha_1 x_m(n-D) e^{j\frac{2\pi}{N}\epsilon n} e^{-j\frac{2\pi}{N}ln}. \end{aligned} \tag{3.9}$$

After substituting $x_m(n)$ and $x_{m-1}(n)$ into (3.9) by using (3.4), and performing proper mathematical operations of which time invariant case is also given in [43], received signal can be partitioned into five parts as

$$\begin{aligned} Y_m(l) =& \frac{1}{N} X_m(l) \left(\alpha_0 \frac{\sin\pi\epsilon}{\sin\frac{\pi}{N}\epsilon} e^{j\pi\epsilon\frac{N-1}{N}} + \alpha_1 \frac{\sin\pi\epsilon\frac{N-D+N_{\mathrm{G}}}{N}}{\sin\frac{\pi}{N}\epsilon} e^{j\left(\pi\epsilon\frac{N-D+N_{\mathrm{G}}}{N} + \frac{2\pi}{N}\epsilon(D-N_{\mathrm{G}}) - \frac{2\pi}{N}lD\right)} \right) \\ &+ \frac{\alpha_0}{N}\sum_{k=0,k\neq l}^{N-1} X_m(k) \frac{\sin\pi(k+\epsilon-l)}{\sin\frac{\pi}{N}(k+\epsilon-l)} e^{j\pi(k+\epsilon-l)\frac{N-1}{N}} \\ &+ \frac{1}{N} X_{m-1}(l) \left(\alpha_1 \frac{\sin\pi\epsilon\frac{D-N_{\mathrm{G}}}{N}}{\sin\frac{\pi}{N}\epsilon} e^{j\left(\pi\epsilon\frac{D-N_{\mathrm{G}}-1}{N} - \frac{2\pi}{N}l(D-N_{\mathrm{G}})\right)} \right) \\ &+ \frac{\alpha_1}{N}\sum_{k=0,k\neq l}^{N-1} X_{m-1}(k) \frac{\sin\pi(k+\epsilon-l)\frac{D-N_{\mathrm{G}}}{N}}{\sin\frac{\pi}{N}(k+\epsilon-l)} \cdot e^{j\left(\pi(k+\epsilon-l)\frac{D-N_{\mathrm{G}}-1}{N} + \frac{2\pi}{N}k(N_{\mathrm{G}}-D)\right)} \\ &+ \frac{\alpha_1}{N}\sum_{k=0,k\neq l}^{N-1} X_m(k) \frac{\sin\pi(k+\epsilon-l)\frac{N-D+N_{\mathrm{G}}}{N}}{\sin\frac{\pi}{N}(k+\epsilon-l)} \\ &\qquad \cdot e^{j\left(\pi(k+\epsilon-l)\frac{N-D+N_{\mathrm{G}}-1}{N} - \frac{2\pi}{N}kD + \frac{2\pi}{N}(k+\epsilon-l)(D-N_{\mathrm{G}})\right)}. \end{aligned} \tag{3.10}$$

First, assume the channel is time invariant, i.e. $\epsilon = 0$. By considering regular subcarrier population, that is, the case in which all subcarriers are populated by nonzero data symbols, the first term in (3.10) is desired signal coming from the first and the second paths of multipath channel. The second term, ICI caused by time variation, disappears when ϵ is set to zero. The third and the fourth terms are $I_{\mathrm{ISI,SC}}$ and $I_{\mathrm{ISI,OC}}$, respectively. The fifth term is due to loss of orthogonality between subcarriers of current symbol ($I_{\mathrm{ICI,LO}}$). Assuming complex symbols on subcarriers are independent and equally likely, expected

power of last two interference components in time invariant channel becomes

$$E(|I_{\mathrm{ISI,OC}}|^2) = \frac{|\alpha_1|^2}{N^2} \sum_{k=0,k\neq l}^{N-1} \left(\frac{\sin \pi(k-l)\frac{D-N_{\mathrm{G}}}{N}}{\sin \frac{\pi}{N}(k-l)} \right)^2 \tag{3.11}$$

$$= E(|I_{\mathrm{ICI,LO}}|^2). \tag{3.12}$$

When we substitute the subcarrier activation as in (3.6), summation of all subcarriers for odd indexed received OFDM symbol yields

$$\begin{aligned}
\sum_{l=0}^{N-1} Y_m(l) =& \left(\alpha_0 + \alpha_1 \frac{N-D+N_{\mathrm{G}}}{N} e^{-j\frac{2\pi}{N}\frac{m-1}{2}D} \right) \\
&+ \alpha_1 \frac{D-N_{\mathrm{G}}}{N} e^{-j\frac{2\pi}{N}\frac{m-1+N}{2}(D-N_{\mathrm{G}})} \\
&+ \frac{\alpha_1}{N} \sum_{\substack{l=0, \\ l\neq \frac{m-1+N}{2}}}^{N-1} \frac{\sin \pi(\frac{m-1+N}{2}-l)\frac{D-N_{\mathrm{G}}}{N}}{\sin \frac{\pi}{N}(\frac{m-1+N}{2}-l)} \\
&\qquad \cdot e^{j\pi(\frac{m-1+N}{2}-l)\frac{D-N_{\mathrm{G}}-1}{N}} e^{j\frac{2\pi}{N}\frac{m-1+N}{2}(N-D+N_{\mathrm{G}})} \\
&+ \frac{\alpha_1}{N} \sum_{\substack{l=0 \\ l\neq \frac{m-1}{2}}}^{N-1} \frac{\sin \pi(\frac{m-1}{2}-l)\frac{N-D+N_{\mathrm{G}}}{N}}{\sin \frac{\pi}{N}(\frac{m-1}{2}-l)} \\
&\qquad \cdot e^{j\pi(\frac{m-1}{2}-l)\frac{N-D+N_{\mathrm{G}}-1}{N}} e^{j\frac{2\pi}{N}\frac{m-1}{2}N_{\mathrm{G}}} e^{j\frac{2\pi}{N}l(D-N_{\mathrm{G}})}
\end{aligned} \tag{3.13}$$

in which the expected interference powers of last two term is the same as in (3.12). This fact also proves that the total interference from one subcarrier to others is the same as total interference experienced by one subcarrier. $I_{\mathrm{ISI,SC}}$ and $I_{\mathrm{ISI,OC}}$ terms in (3.13) emerge as a hill at $N/2$ subcarrier distance with active subcarrier index as in Figure 3.5(b) and Figure 3.5(c). Also, the third term in (3.13), which is $I_{\mathrm{ICI,LO}}$, appears near the active subcarrier location.

In the presence of both time selectivity and insufficient CP size, ICI power due to the time selectivity, $I_{\mathrm{ICI,TS}}$, combines with the $I_{\mathrm{ICI,LO}}$ in the interference spectrogram which can be observed in Figure 3.6(a). $I_{\mathrm{ICI,TS}}$ is dominant at the subcarriers near the active subcarrier because the second term in (3.10) emerges and equality of the fourth and

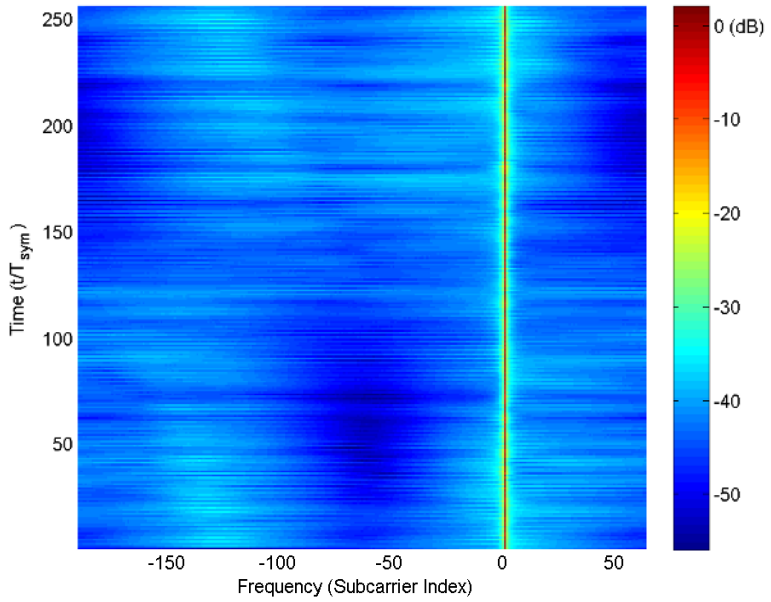

(a) Insufficient CP size with Doppler spread

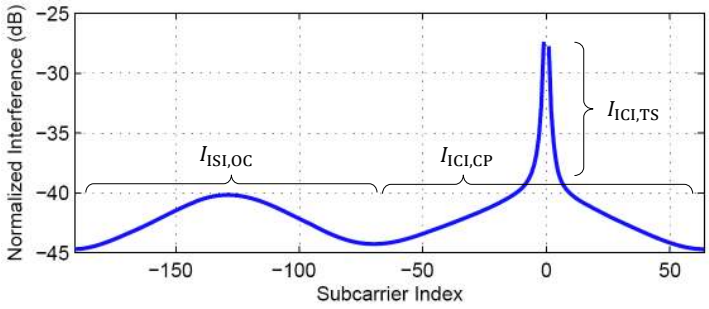

(b) Averaged spectrogram over time axis.

Figure 3.6 (a) Interference spectrogram with short CP size as well as Doppler spread and (b) corresponding self interferences.

the fifth terms in (3.10) for time-invariant case does not hold when the channel is time varying. Further to that, the magnitudes of the fifth term becomes significantly larger then the fourth term as

$$\left|\frac{\sin\pi(k+\epsilon-l)\frac{D-N_{\mathrm{G}}}{N}}{\sin\frac{\pi}{N}(k+\epsilon-l)}\right| \ll \left|\frac{\sin\pi(k+\epsilon-l)\frac{N-D+N_{\mathrm{G}}}{N}}{\sin\frac{\pi}{N}(k+\epsilon-l)}\right|, \epsilon \notin \mathbb{Z}, \tag{3.14}$$

especially for small subcarrier distances $k-l$, dominating the overall summation over $\{k : k \in \{0,1,...,N-1\}, k \neq l\}$. This relationship can also be also observed in Figure 3.7.

Both left and righ hand sides of the (3.14) is plotted as a function of subcarrier distance for $N = 256$, $D - N_{\mathrm{G}} = 3$, and $\epsilon = 0.1$. Inequality in (3.14), i.e., dominating effect in Figure 3.7, corresponds to fact that additional interference due to the time selectivity on $I_{\mathrm{ISI,OC}}$ is negligible compared to that of $I_{\mathrm{ICI,LO}}$. The reason is that the durations of the previous symbol's multipath components in DFT window are very small relative to those of current symbol's multipath components.

Similarly, time variation effect on $I_{\mathrm{ISI,OC}}$ is negligible when $\frac{D-N_{\mathrm{G}}}{N} \ll 1$. In other words, when we remove the time variation from $I_{\mathrm{ISI,OC}}$ term, we observe that

$$\left| \frac{\sin \pi(k-l)\frac{D-N_{\mathrm{G}}}{N}}{\sin \frac{\pi}{N}(k-l)} \right| \backsimeq \left| \frac{\sin \pi(k+\epsilon-l)\frac{D-N_{\mathrm{G}}}{N}}{\sin \frac{\pi}{N}(k+\epsilon-l)} \right|, \tag{3.15}$$

which can also be observed from Figure 3.7.

3.3.3 Interference Separation

Until this point, we analyzed the relations between interferences when multiple sources exist, as well as their visualizations. Based upon the (3.14) and (3.15), we can conclude that interference due to time selectivity is localized near the active subcarrier line, i.e., the right half of the Figure 3.6(b). Furthermore, given that expected powers of two components of ISI are equal as in (3.12), $I_{\mathrm{ICI,TS}}$ can be differentiated from ICI due to insufficient CP by subtracting total power of farthest $N/2-1$ subcarriers to the active subcarrier from total power of closest $N/2-1$ subcarriers to the active subcarrier as

$$\hat{P}^{k}_{\mathrm{ICI,TS}} = \underbrace{\sum_{\substack{l=k-N/4, \\ l\neq k}}^{k+N/4-1} |Y(l)|^2}_{I_{\mathrm{ICI,TS}}+I_{\mathrm{ICI,LO}}} - \underbrace{\sum_{\substack{l=k-3N/4, \\ l\neq k-N/2}}^{k-N/4-1} |Y(l)|^2}_{I_{\mathrm{ISI,OC}}}. \tag{3.16}$$

(3.16) gives the ICI originated by time selectivity for the OFDM symbol in which kth subcarrier is activated. Expected value of power of $I_{\mathrm{ICI,TS}}$ is then estimated by averaging

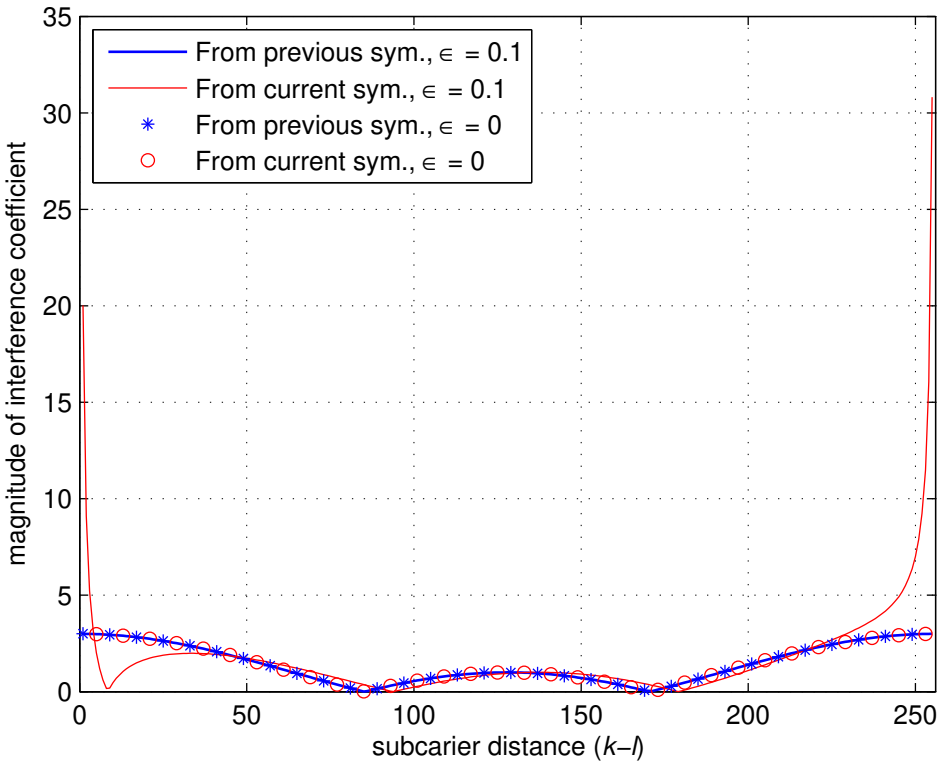

Figure 3.7 Interference contributions from previous and current symbol. Time variation effect of multipath component of current symbol dominates that of previous symbol. Also, effect of time variation on previous symbol's multipath component is negligible since the duration inside the DFT window is relatively short.

over N symbols in the received frame as

$$\hat{P}_{\mathrm{ICI,TS}} = \frac{1}{N} \sum_{k=0}^{N-1} \hat{P}^{k}_{\mathrm{ICI,TS}}. \tag{3.17}$$

3.3.4 Effect of Frequency Offset

As a time varying impairment, frequency spreading has random behavior. In other words, a single tone spreads along frequency with the power density according to Jakes' Model [44] in a time varying Rayleigh fading multipath channel in which angles of incoming rays are uniformly distributed. However other time varying impairment, CFO, can be assumed to have a deterministic behavior in the time range under consideration because the local oscillator frequencies of the transmitter and receiver are static. Thus, being de-

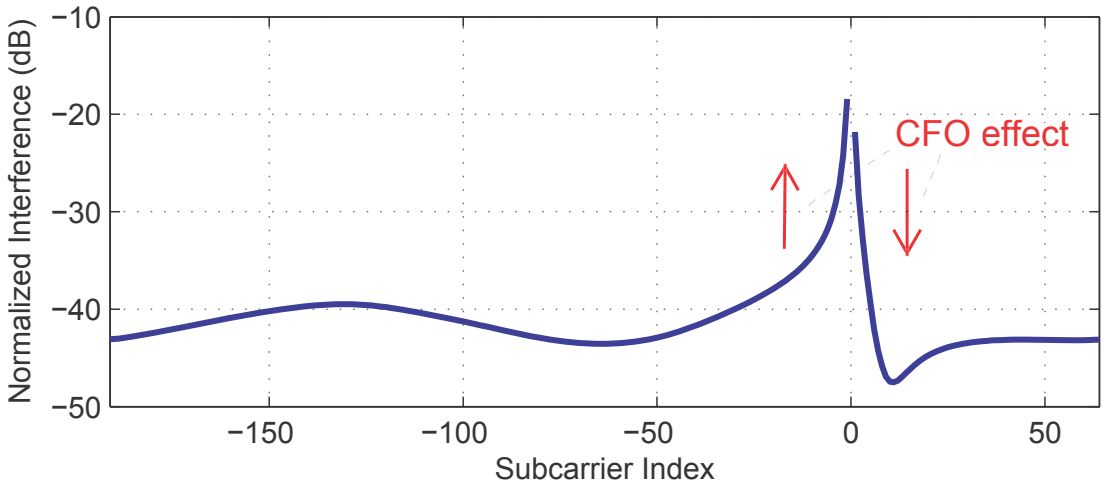

Figure 3.8 Time-averaged spectrogram with insufficient CP size and CFO.

terministic effect, CFO can be identified from the interference spectrogram. For instance, interference spectrogram when both insufficient CP size and CFO exist is given in Figure 3.8. Multipath components of current symbol which has longer excess delay than the CP duration have naturally shorter durations than T_{U} in the receiving window. This results in expanded sinc-shaped subcarriers, i.e., zero crossings of the sinc-shaped subcarriers occurs at frequencies greater than $\Delta f = 1/T_{\mathrm{U}}$. Therefore, CFO contributes to expanded subcarriers constructively at one side of active subcarrier and destructively at the other side which leads to asymmetric profile of the interference near the active subcarrier. This can be observed from Figure 3.8 in which CFO. Asymmetric behaviour in the interference spectrogram can also be used to differantiate between two time varying impairments, frequency spreading and CFO, which is also investigated by frequency domain eye diagram in Section 4.

3.4 Results

3.4.1 Simulation Results

Estimation performances for interferences with proposed method are tested via Monte Carlo simulations. International Telecommunication Union (ITU) vehicular channel B model [45] is used for multipath channel impulse response along with various maximum

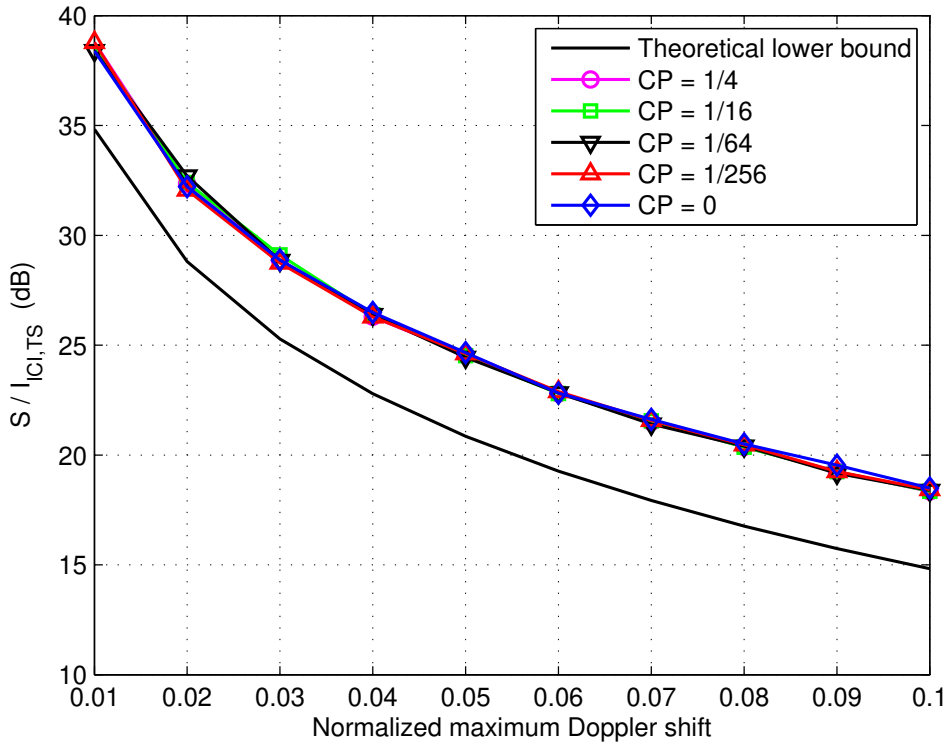

Figure 3.9 Estimated and theoretical $S/I_{\mathrm{ICI,TS}}$ with both multipath channel with different Doppler spreads.

Doppler shifts. Subcarrier spacing, Δf, and number of subcarriers, N, are chosen as 15 kHz and 256, respectively. 500 OFDM frames are generated and processed for each simulation result. First, we investigate signal to $I_{\mathrm{ICI,TS}}$ ratio as a function of maximum Doppler shift, whose estimation performance is given in Figure 3.9. Different CP sizes are adopted in order to have various multipath-caused ISI and ICI. In Figure 3.9, same results for $S/I_{\mathrm{ICI,TS}}$ with different CP sizes show that existing interference because of insufficient CP size does not affect the performance of $I_{\mathrm{ICI,TS}}$ estimation. In other words, interference caused by time variance is separated from the interference caused by insufficient guard period. There exists around 4 dB offset between estimated values and theoretical curve, universal bound for ICI power [46], because the universal bound corresponds to worst case in which all spectral components are assumed to have maximum Doppler shift.

For the same simulation setup, estimation performance of multipath-caused interference is examined. Figure 3.10 shows the $S/(I_{\mathrm{ISI,SC}}+I_{\mathrm{ISI,OC}}+I_{\mathrm{ICI,LO}})$, i.e., signal to total

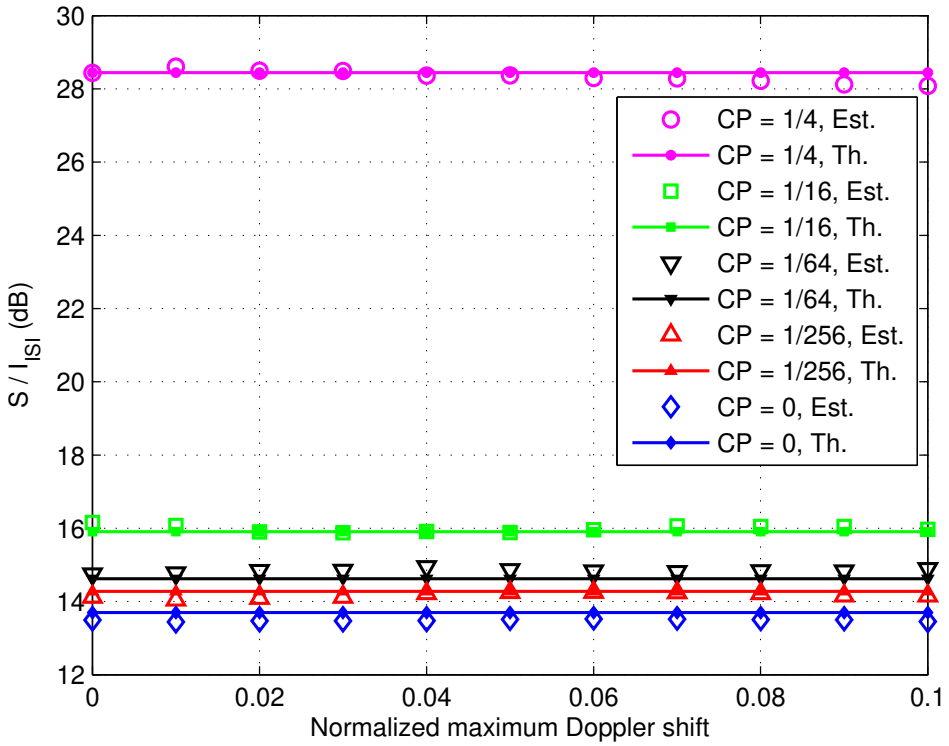

Figure 3.10 Estimated and theoretical $S/(I_{\mathrm{ISI,OC}} + I_{\mathrm{ISI,SC}} + I_{\mathrm{ICI,LO}})$ in multipath channel with different Doppler spreads and CP sizes.

interference caused by insufficient CP ratio, for various time variation scenarios. Similar to previous observation, the same estimation results along different time variations is observed. This validates the approximations done in the method. Interference estimation is critical in noisy channel conditions. We also investigate the interference powers for various signal-to-noise ratio (SNR) conditions. Figure 3.11 shows signal to inter-symbol interference powers versus SNR for different CP sizes. As can be deduces from the figure, estimation results follow the theoretical values when interference power exceeds the noise power, and accuracy of the method degrades as the SNR decreases because high noise power dominates the interference to be measured.

3.4.2 Efficiency of the Method

One frame consists of N symbols by also considering the spectrogram construction as an interference visualization tool. In addition to that, summation of $N-1$ subcarriers

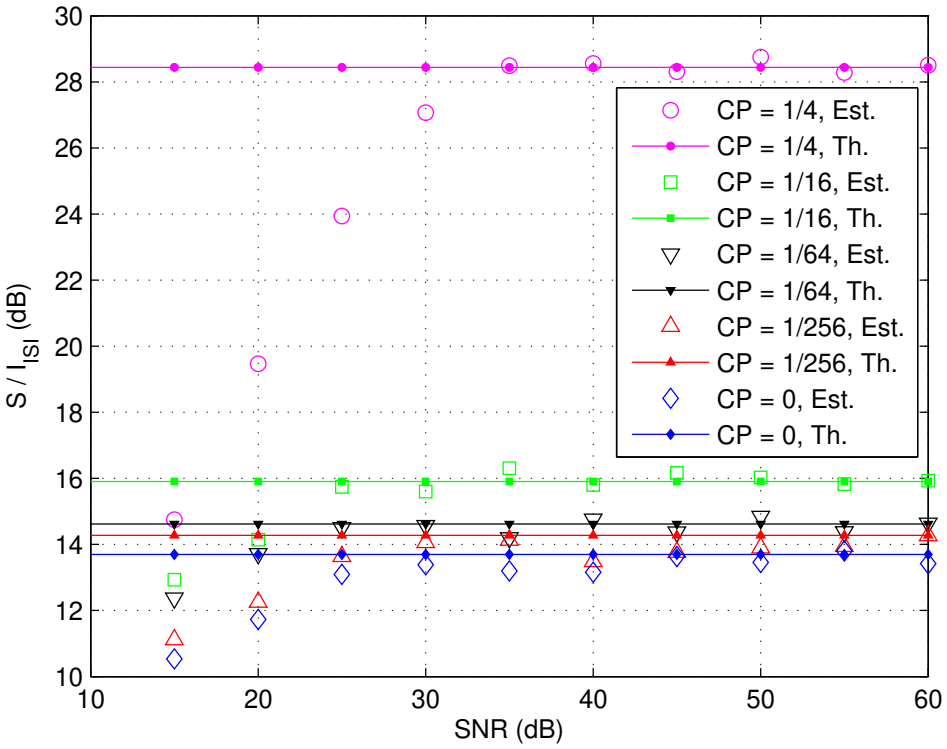

Figure 3.11 Estimated and theoretical $S/(I_{\mathrm{ISI,OC}} + I_{\mathrm{ISI,SC}} + I_{\mathrm{ICI,LO}})$ in multipath channel with different SNR values.

for ISI measurement averages the frequency selectivity of the multipath channel. Number of symbols in the designed frame can be reduced by increasing the step size of the sub-carrier indexes of consecutive symbols to decrease the resource allocated for interference identification procedure in the system. Therefore, increasing the efficiency might trade the estimation accuracy. ISI estimation performance is investigated for various step sizes. Table 3.1 includes absolute estimation errors relative to the case in which $N-1$ symbols are utilized when maximum Doppler shift is set to . The error increases as less number of symbols in the frame is used.

3.4.3 Measurements

Interference identification method is tested in wireless communication systems laboratory in order to confirm the practical implementation and utility under real channel conditions. Laboratory setup for the measurements is illustrated in Figure 3.12. Baseband

Table 3.1 Estimation error as a function of step size.

Step size	Absolute error in I_{ISI} est. (dB)	Absolute error in $I_{\mathrm{ICI,TS}}$ est. (dB)
2	0.107	0.225
4	0.168	0.241
8	0.305	0.426
16	0.412	0.654
32	0.735	0.847
64	1.009	0.850
128	1.473	1.571

OFDM frames are generated in software and pushed to the Agilent E4438C ESG vector signal generator (VSG) over the local area network (LAN). VSG upconverts the baseband signal to the radio frequency (RF) and pushes it to the antenna. Then, transmitted signal passes through the wireles channel. The signal is captured by Agilent E4440A PSA vector signal analyzer (VSA) and interference calculations are performed in the software. Frame and symbol synchronization is achieved via trigger connection from VSG to VSA to prevent undesired timing offset. Also, in order to avoid undesired (and unknown) frequency offset between local oscillators, VSG is driven by VSA's carrier frequency reference.

It is not possible to create a time varying channel in wireless communication laboratory with known characteristics for validation of the estimation method. Thus, CFO, whose theoretical characteristics is known, is adopted for inserting time variation into the wireless channel. Intentional CFO is inserted by manipulating the carrier frequency of the VSA. Figure 3.13 shows the theoretical, estimated and measured $S/I_{\mathrm{ICI,TS}}$ values with CP sizes of $N/4$ and 0. Estimation results match with theoretical and measurement results confirming the effectiveness and implementation of the proposed method in practice.

Finally, ISI estimation performance is investigated via measurements. Similar to previous case, intentional timing offset is inserted for each case in order to be able to have a theoretical reference. Theoretical, simulation, and measurement results for $S/(I_{\mathrm{ISI,SC}} + I_{\mathrm{ISI,OC}} + I_{\mathrm{ICI,LO}})$ is given in Figure 3.14 as a function of timing offset between transmission and reception, i.e., delay in the channel. While simulation results match the theory, measurement results has some error due to practical problems possibly related to the setting the exact timing instant.

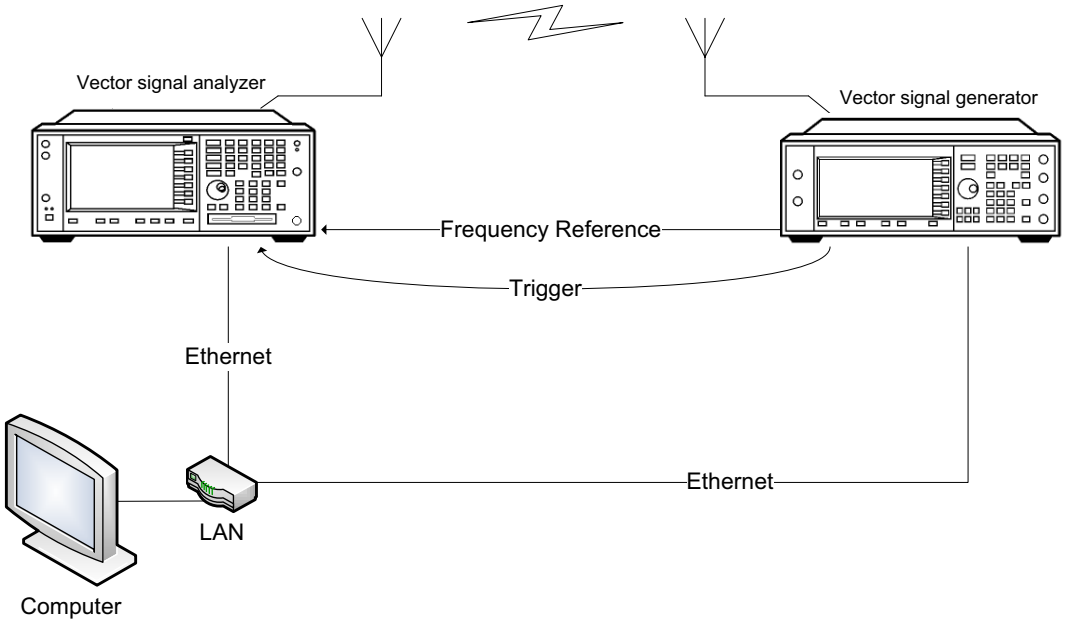

Figure 3.12 Laboratory setup for interference measurements.

3.5 Conclusions

A test and measurement method focusing on interference identification, which allows better interference management for OFDM based communication systems, is studied. Instead of considering total or average interference that the signals are exposed to, the interference contributions from different impairments are separated with the proposed method. Constructed interference spectrogram driven by received OFDM symbols visualizes other user's interferences like NBI and ACI with spectrogram nature of diagram as well as self interferences caused by insufficient CP, time selectivity explicitly. Powers of different interferences are obtained with reasonable estimation errors. Along with simulations, the method is also validated with the measurements in the wireless communication laboratory. With proposed scheme, better understanding of the interference sources in OFDM based communication systems is obtained, which can be used for testing, interference measurement, and educational purposes.

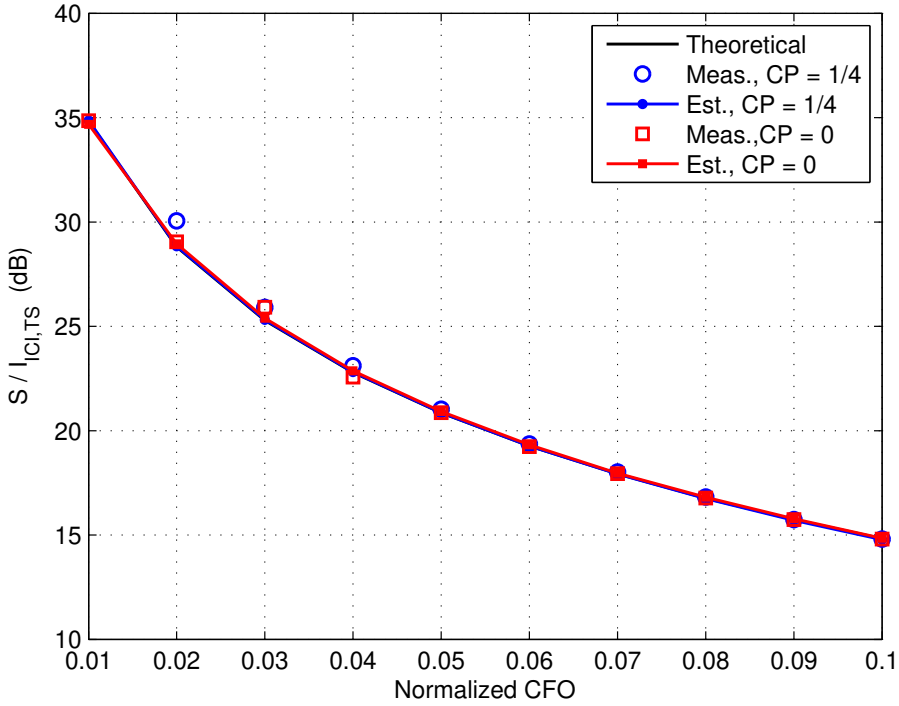

Figure 3.13 Theoretical, estimated and measured $S/I_{\mathrm{ICI,TS}}$ in multipath channel with different Doppler spreads and CP sizes.

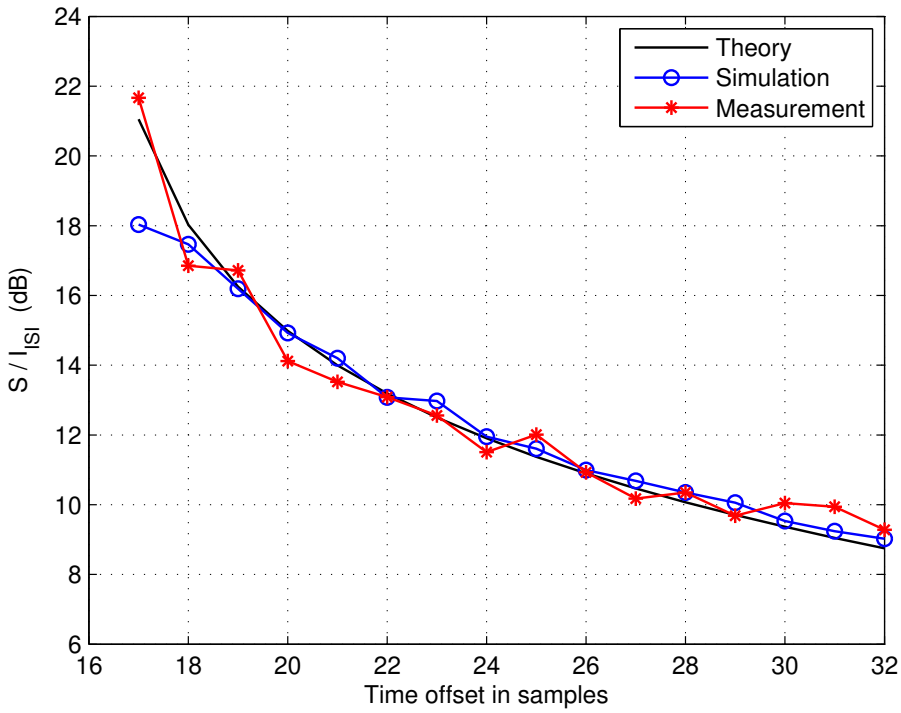

Figure 3.14 Theoretical, simulated, and measured S/I_{ISI} with different timing offsets.

CHAPTER 4:
FREQUENCY DOMAIN EYE DIAGRAM FOR OFDM

4.1 Introduction

In wireless communications, information is represented by various types of parameters in various types of dimensions of the electro space. In general, the operation of mapping the analog or digital information to the fundamental dimensions of the communication signal like frequency, phase, amplitude etc. is called as modulation. In addition to main dimensions, artificial domains in the electro space like spreading and hopping sequence can be used for data transmission.

Orthogonal frequency-division multiplexing (OFDM) has been adopted by wireless communication systems because of its ability to effectively convert frequency selective channel to multiple flat subchannels that can easily be handled by one tap frequency domain equalization [47], adaptive and flexible bandwidth utilization [48], and higher spectral efficiency with overlapping subcarriers. Despite the prominent advantages in time dispersive channels, high spectral sidelobes of overlapping subcarriers make OFDM sensitive to intercarrier interference (ICI) in the presence of time varying channel. In other words, frequency spreading due to mobility of transmitter, receiver, or the physical environment in between leads to interference between subcarriers. Also, hardware based time varying impairments like carrier frequency offset (CFO) and phase noise ruin the orthogonality of the subcarriers resulting in the ICI.

Baseband symbols in wireless communications are defined in various dimensions in which transmit channel has different effects. Identification of impairment source is critical for complete system analysis. Therefore, in testing and measurements, channel impact on signals in different dimensions should be considered. For example, eye diagrams have been

Table 4.1 Impairments by domain and source. Frequency domain eye diagram is to observe time varying impairments.

		Domain	
		Time	**Frequency**
Source	**Channel**	Delay spread	Frequency spread
	Hardware	Timing jitter	Carrier frequency offset
Visualization		Time Domain Eye Diagram	Frequency Domain Eye Diagram

heavily used to observe the impairments in single carrier systems such as Global System for Mobile Communications (GSM) in which the symbols are defined in time domain. However in OFDM based systems, transmitted symbols are modulated along subcarriers that are defined in frequency domain. Therefore, an eye diagram in frequency domain for OFDM subcarriers can be used as a tool to achieve the detection and visualization of the time varying channel impairments while inter-symbol interference caused by channel impairments like delay spread and timing jitter for single carrier signals is observed by time domain eye diagram.

Use of eye diagrams for communication signals in time domain is extensively discussed in [49] and eye pattern is introduced for noncoherent receivers including estimation of required carrier to noise ratio for required error rate in [50]. Time domain eye diagram is a powerful tool to investigate interference between consecutive time domain symbols. Overlapping of OFDM subcarriers in frequency is analogous to time overlapping of Nyquist pulses in single carrier communications. For example, raised cosine filter is the popular pulse shaping filter that satisfies the Nyquist criterion [51]. However, zero-inter-symbol interference (ISI) property of Nyquist pulse shaped single carrier signals is distorted in multipath channels. Timing jitter at the receiver also causes ISI. Similar to impact of channel impairments like delay spread and timing jitter on zero-ISI property of Nyquist filtered single carrier signals, time varying channels disturb the zero-ICI property of the OFDM subcarriers.

Inspired by this analogy, frequency domain eye diagram (FDED) is introduced in order to investigate such distortions as frequency spread and CFO as summarized in Table 4.1.

The use of FDED in testing and validation of the software defined radio systems provides useful information whether carrier frequency offset and frequency spreading occur or not by considering shift of eye crossings and reduced eye openings in the analysis, respectively. Frequency offset estimation without utilizing preambles is also possible by determining the shift of eye pattern that minimizes the error magnitude of interpolated points. Also, as a visualization tool, the technique can be implemented for educational purposes.

This chapter is organized as follows: In Section 4.2, system model is introduced. Section 4.3 demonstrates signal generation and construction of FDED with examples. Measurement results for various channel scenarios are given in Section 4.4. Finally, conclusions are drawn in section 4.5.

4.2 System Model

We consider an OFDM system in which transmitter generates symbols by processing complex baseband symbol vector with centered inverse discrete Fourier transform (IDFT) operation. Since the time indexes of regular IDFT and discrete Fourier transform (DFT) operations are defined from zero to $N-1$, zero padding in time distorts the symmetric property of transform pairs which results in complex interpolation between DFT points. Rotation of interpolated samples prevents to obtain clear eye patterns for OFDM subcarriers. In order to avoid the complex interpolation, centered DFT is implemented for OFDM signal generation and reception, that also provides full analogy with continuous Fourier transform [52]. After the addition of cyclic prefix (CP), the OFDM symbol is converted to an analog time-domain signal before being transmitted through channel. The sampled time-domain baseband representation for one OFDM symbol at the transmitter becomes

$$x(n) = \sum_{k=-\frac{N-1}{2}}^{\frac{N-1}{2}} X(k) e^{j\frac{2\pi}{N}kn}, \qquad n = -N_{\mathrm{CP}} - \frac{N-1}{2}, \ldots, \frac{N-1}{2} \tag{4.1}$$

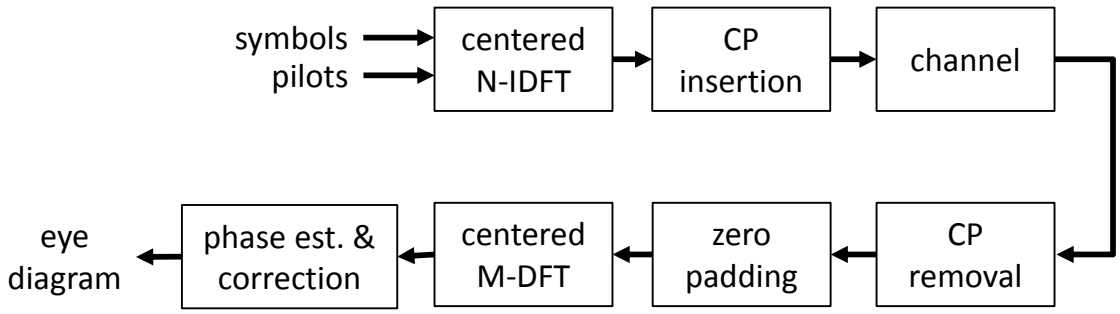

Figure 4.1 Block diagram for frequency domain eye diagram.

where n is sampled time index, $X(k)$ is complex data symbol assigned to kth subcarrier, N is IDFT size which is also number of subcarriers, N_{CP} is CP size in DFT samples and j is imaginary unit.

4.3 Frequency Domain Eye Diagram

DFT operation at the OFDM receiver corresponds to rectangular receiver filtering. In other words, after correct time synchronization and removing CP, kth element of DFT output vector corresponds to receiver filter output sampled at the correct time for kth subcarrier. Eye diagram is constructed by having denser interpolation between DFT output samples at the receiver. By zero padding to the sampled received signal and performing greater size centered DFT, sinc-interpolation between the subcarrier data is performed, which is inherently the shape of the subcarriers. By so doing, the analysis operation, DFT, approaches to discrete-time Fourier transform (DTFT) as illustrated in Figure 4.2. Although time range should extend from $-\infty$ to ∞ to get the exact DTFT, padding finite number of zeros in time signal is sufficient for performing interpolation to get eye diagram. Figure 4.1 shows block diagram for OFDM system with eye diagram construction.

At the receiver end, CP is removed from the received OFDM symbols after passing through the channel. Then, zero padding and centered DFT are performed in the reception

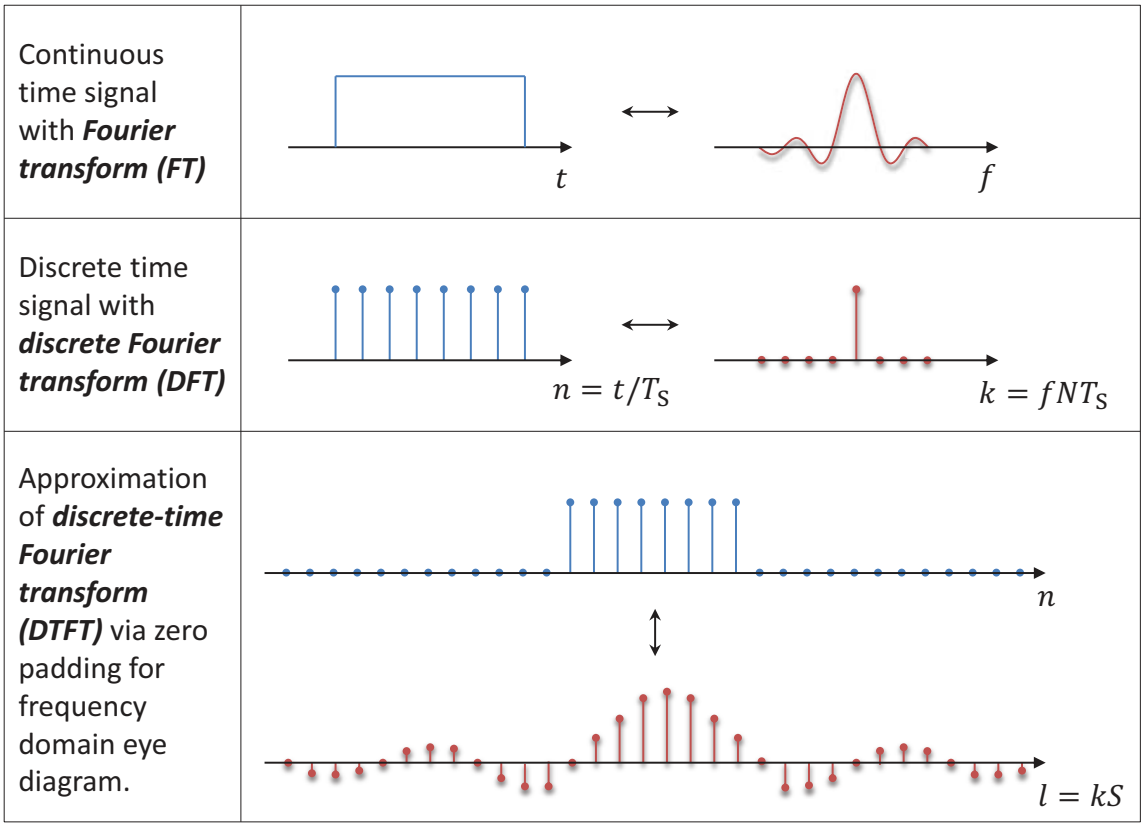

Figure 4.2 Transform pairs including FT, DFT, and DTFT approximation for FDED.

stage as follows

$$X_{ip}(l) = \sum_{m=-\frac{M-1}{2}}^{\frac{M-1}{2}} x_{zp}(m) e^{-j\frac{2\pi}{M}lm}, \qquad l = -\frac{M-1}{2}, \ldots, \frac{M-1}{2} \tag{4.2}$$

where l is index of interpolated frequency components of received OFDM signal, $M \geq N$ is DFT size and m is sampled time index of the zero padded signal

$$x_{zp}(m) = \begin{cases} 0, & -\frac{M-1}{2} \leq m < -\frac{N-1}{2} \\ x(m), & -\frac{N-1}{2} \leq m \leq \frac{N-1}{2} \\ 0, & \frac{N-1}{2} < m \leq \frac{M-1}{2}. \end{cases} \tag{4.3}$$

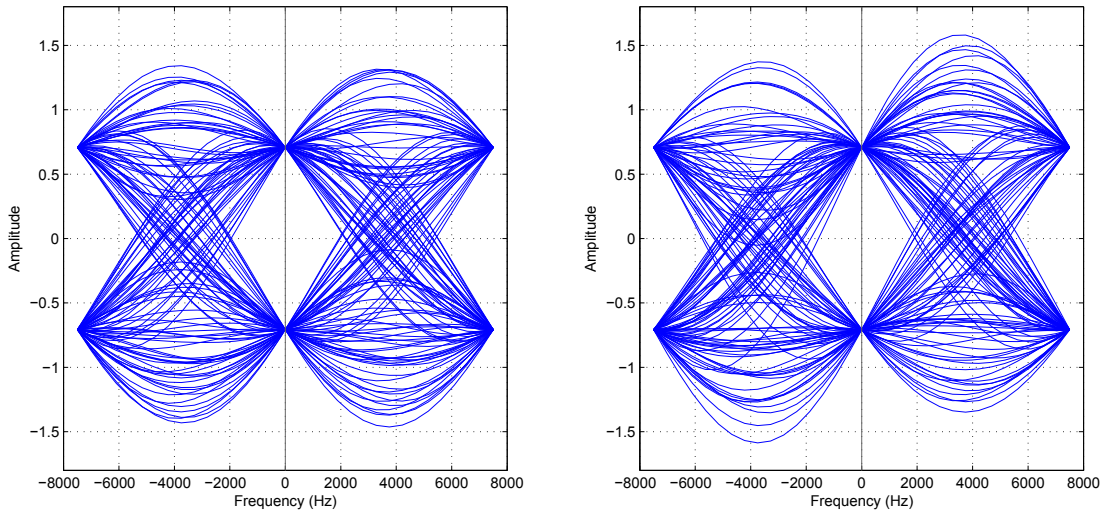

(a) (b)

Figure 4.3 Simulated frequency domain eye diagrams for (a) in-phase and (b) quadrature component without impairment.

Interpolated frequency domain OFDM symbols are used to construct eye patterns. As the greater DFT size is achieved at the receiver, eye diagram for both in phase and quadrature part of complex baseband symbols are constructed via partitioning the interpolated frequency domain symbols into two carrier spacing-sized chunks. Then, each chunk is plotted at the top of each other to construct the eye diagrams. At the final step, two diagrams are obtained for each symbol: Real part of complex subcarriers, $\Re\{X_{ip}(l)\}$, is for eye diagram of in-phase component of the symbols which are modulated on subcarriers while imaginary part, $\Im\{X_{ip}(l)\}$, is for eye diagram of quadrature component. Figure 4.3(a) and Figure 4.3(b) show the simulated eye diagrams for in-phase and quadrature components, respectively. quadrature phase-shift keying (QPSK) symbols are generated without channel effect along with $N = 256$, $M = 4096$, and 7.5 kHz subcarrier spacing.

4.3.1 Effect of Frequency Selectivity

FDED is considered to observe the time-varying impairments. However in highly frequency-selective channels, plotting N subcarriers on top of each other to obtain the eye pattern distorts eye openings. Since the subcarriers are filtered with different channel

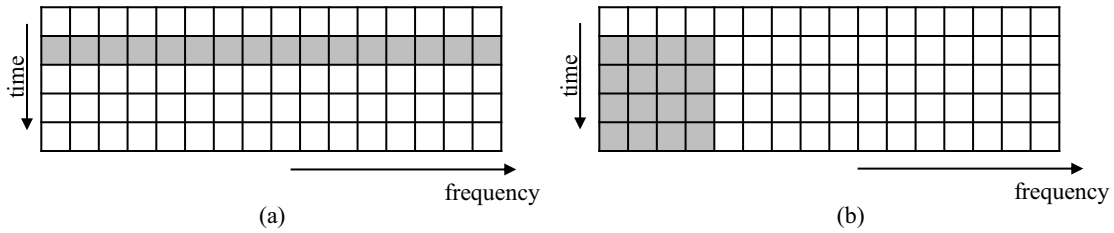

Figure 4.4 Changing the map for used subcarriers to mitigate frequency selectivity.

amplitude and phase responses along frequency, contribution of each subcarrier to the eye digram is effected by delay spread rather than time selectivity. Therefore, in order to mitigate the effect of frequency selectivity on eye patterns, number of subcarriers in each OFDM symbol used to construct FDED is reduced while consecutive symbols are included in diagram construction as illustrated in Figure 4.3.1.

4.4 Simulations and Measurements

Due to the physical limitations in the wireless communications laboratory, multipath channel with long delay spread is hard to generate. Therefore, effect of frequency selectivity has been investigated via software simulations while time varying impairments are tested in the wireless communications laboratory.

For simulations, ITU Pedestrian A multipath channel model is adopted [45]. Subcarrier spacing is set as 7.7 kHz with $N = 128$. In order to mitigate the effect of frequency selectivity, $N/4$ subcarriers of 4 symbols, keeping number of total components the same, are utilized for plotting the eye diagram. Two knobs at each sampling point of subcarriers are observed in Figure 4.4 because of different channel gains at frequencies corresponding to the those subcarriers. Figure 4.4 shows the effect of Doppler spread in the channel.

FDED is tested in wireless communication systems laboratory in order to confirm the in practical utility under real channel conditions. Baseband OFDM signal is generated in software and pushed to the Agilent E4438C ESG Vector Signal Generator. Transmitted signal is captured by Agilent E4440A PSA Spectrum Analyzer after passing through wireless channel. Received signal is downloaded to the computer and FDED is constructed

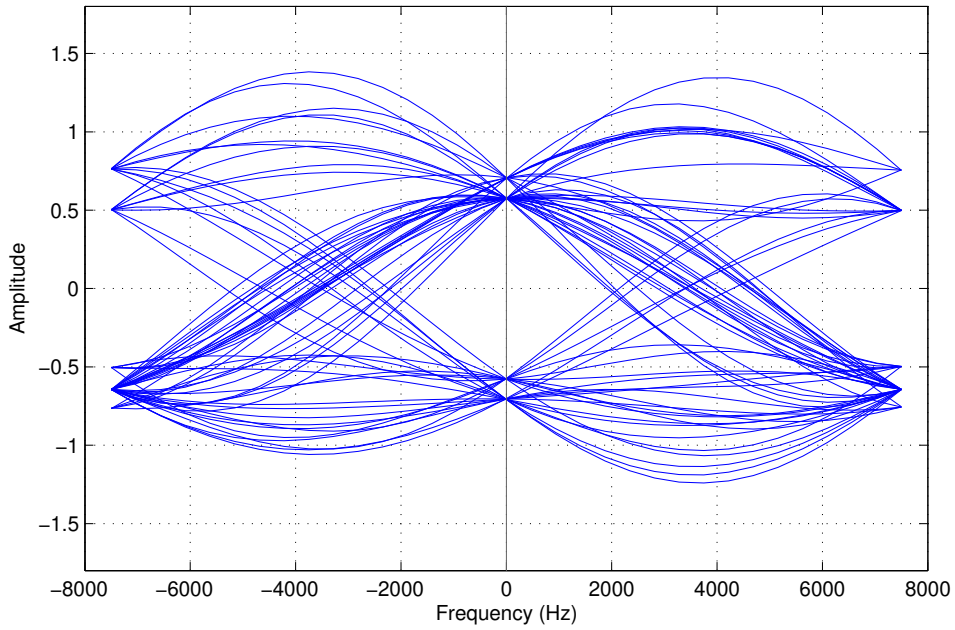

Figure 4.5 Eye diagrams of 4 subcarriers and N/4 symbols without Doppler effect in multipath channel.

in the software. Intentional CFO is inserted by manually changing carrier frequency of the spectrum analyzer and time variation is achieved by putting a rotating fan between transmitter and receiver antennas with a setup as shown in Figure 4.7.

Subcarrier spacing and number of subcarriers are set to 7.5 kHz and 256 in the measurements. To have smooth diagram, interpolation ratio, M/N, is selected as 16 which corresponds to 15 additional eye pattern samples for each DFT sample. Eye diagram for in-phase component of QPSK modulated OFDM signal is given in Figure 4.4, without impairment in the channel. Since the main consideration is time varying impairments, OFDM signal is tested in the presence of time variation in the channel, as well as CFO. For all measurements, common oscillator is used for transmitter and receiver in order not to have uncontrolled frequency offset between local oscillators. For frequency offset measurement, intentional 200 Hz CFO is created at the receiver. Introduced frequency offset is clearly observed as in Figure 4.4. Frequency offset estimation can be performed by minimizing the error magnitude of interpolated subcarriers and with image processing tools, which is out of scope of this study. Time selective channel is carried out by placing a rotating 3-blade

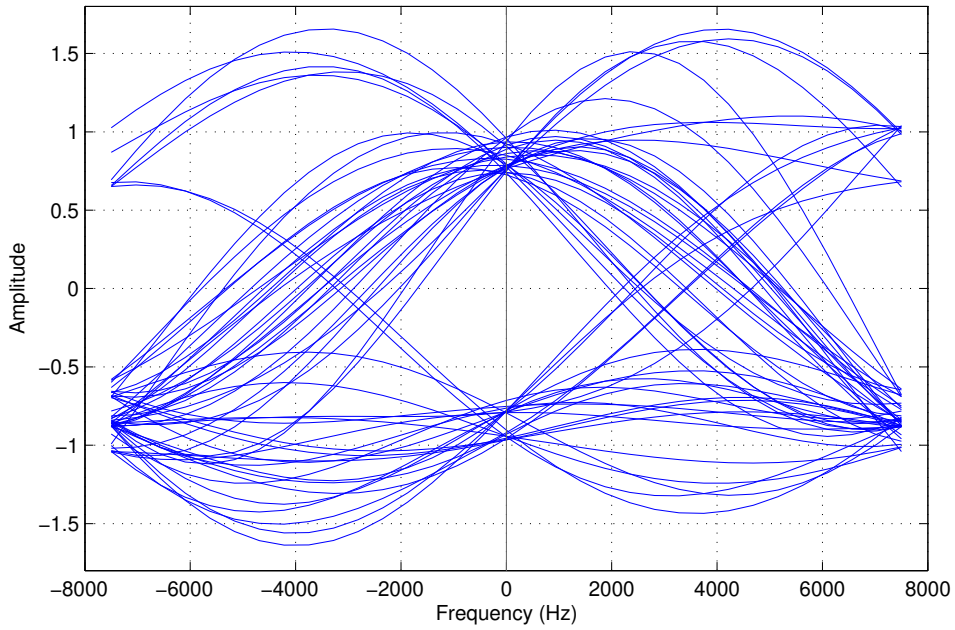

Figure 4.6 Eye diagrams of 4 subcarriers and N/4 symbols with Doppler effect in multipath channel.

fan between transmitter and receiver antennas. Figure 4.4 shows the measured eye diagram when the fan is operating, i.e. creating a time varying channel. Spread in the frequency is observed as distortion in the eye diagram in both directions along frequency. Presence of both CFO and Doppler spread is also investigated. When Doppler spread and CFO occur at the same time, distorted eye diagram shifts with the amount of frequency difference between transmitter and receiver as in Figure 4.11, which also makes frequency offset estimation in time variation possible.

4.5 Conclusions

FDED has been defined for subcarriers of OFDM signals. As time domain eye diagram is used for understanding the impact of impairments on the single carrier waveforms that are transmitted in time domain, time varying impairments like frequency spread and CFO in multicarrier waveforms where the transmitted symbols are defined in frequency domain are visualized and identified from each other with eye patterns in frequency. Proposed method also provides frequency offset estimation without using preamble. FDEDs

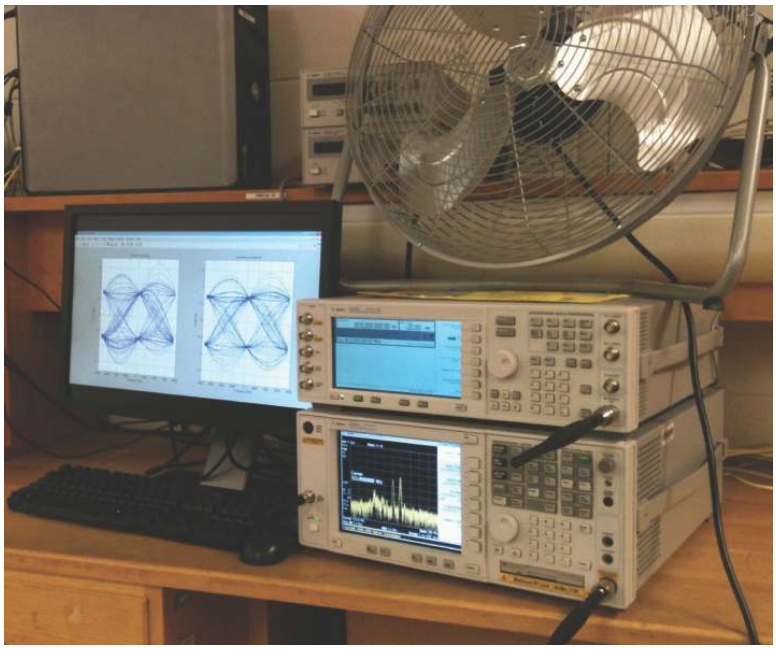

Figure 4.7 Laboratory setup for eye diagram measurements.

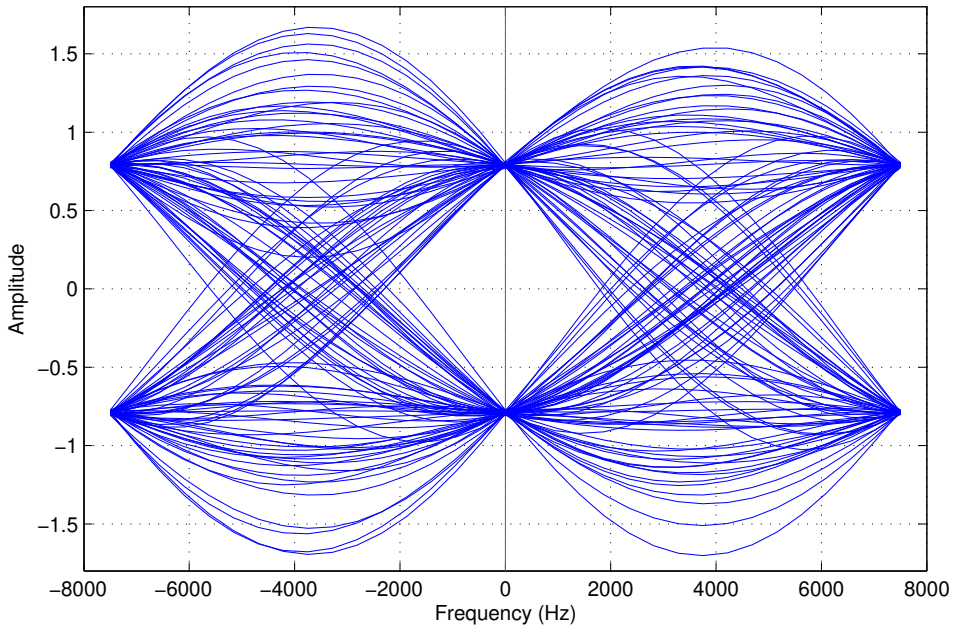

Figure 4.8 Measured eye diagram for in-phase component without impairment.

can be used for testing of OFDM systems, for conducting interference measurements and for educational purposes.

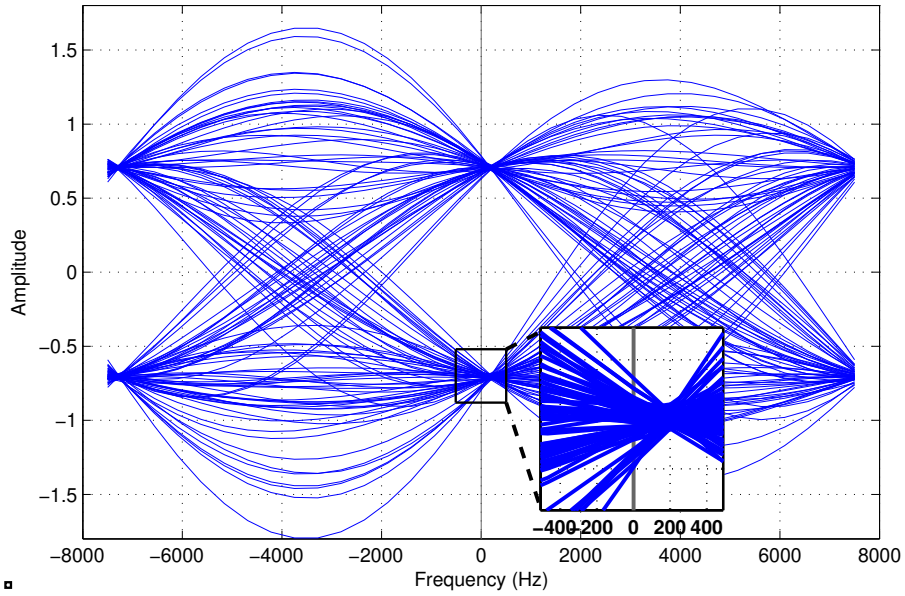

Figure 4.9 Measured eye diagram for in-phase component with 200 Hz intentional CFO.

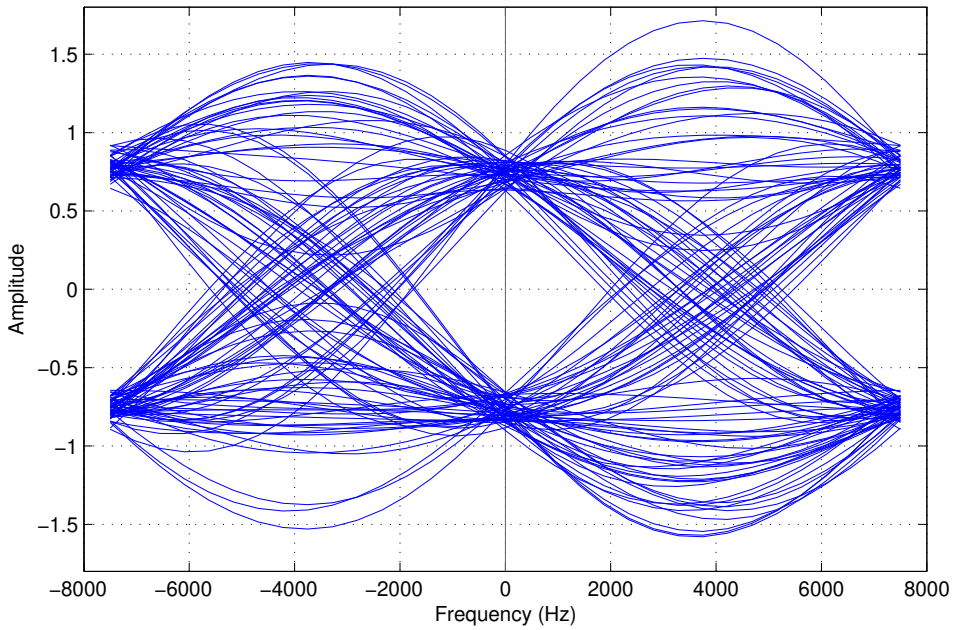

Figure 4.10 Measured eye diagram in the presence of frequency spread with rotating fan.

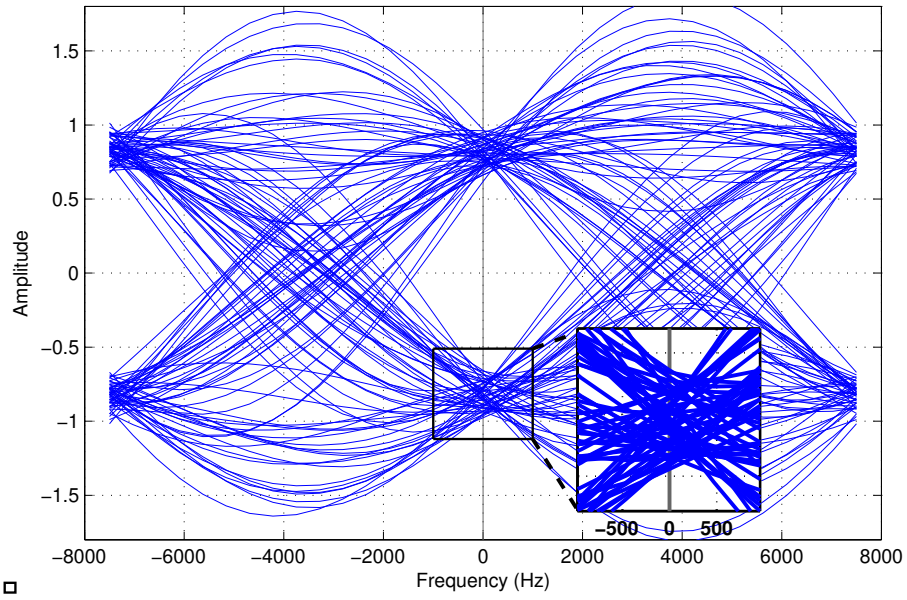

Figure 4.11 Measured eye diagram when both CFO and frequency spread occur.

CHAPTER 5:

CONCLUSION

Increasing demand for high data rate in wireless communications has led to use of wider frequency bands. Conveying the data on single carrier with high symbol rate is limited due to complexity of the equalizing the wideband signal that is affected by frequency-selective channel. With multicarrier communication, on the other hand, equalization cost reduced by dividing the wideband channel into smaller subchannels with flat frequency response. Orthogonal frequency-division multiplexing (OFDM), widely adopted multicarrier scheme, combines the advantages of multicarrier communication and frequency domain equalization. Along with its prominent advantages, multipath and time varying channel along with hardware impairments in OFDM systems cause interference degrading the received signal quality. Although impact of each specific impairment on OFDM and corresponding countermeasure are well known, interference source in the system needs to be identified before performing associated adaptation, or in the test and measurement stage.

In this thesis, methods for identifying, visualizing, and separating the various type of interferences in OFDM systems have been studied. A special OFDM waveform, and interference spectrogram to be used with designed waveform is developed. With introduced method, investigating and visualizing narrowband, adjacent-band, intersymbol and intercarrier interferences is performed with single diagram. Also, identification of different problems such as insufficient guard time and time variance in the channel that result in same consequences at the receiver is performed as well as interference powers are separated when multiple of the aforementioned problems are present. Estimation performance of the proposed methods is tested and validated via computer simulations as well as measurements conducted in the wireless communication laboratory.

As OFDM is quite sensitive to time varying impairments, identification between time varying channel impairments such as frequency offset between local oscillators and frequency spread due to mobility is concentrated further. For this purpose, eye diagram in frequency domain that shows the transitions between OFDM subcarriers is constructed. By using the eye diagram along frequency, the source of inter-carrier interference is identified whether it is frequency offset or spread, which is analogous to investigating multipath channel impairments in single carrier signals with time domain eye diagram. The effectiveness of the introduced diagram is also investigated with simulations and measurements in the presence of corresponding impairments.

Interference awareness is important concept for future communication applications that are excepted to be highly adaptive. By identifying the type and the source of the interference, confidence for action to cope with interference is increased. The proposed methods and results can be utilized for interference awareness in OFDM-based wireless communication systems. Also, methods and diagrams can be used for testing the wireless systems, interference measurements, and educational purposes.

REFERENCES

[1] J. W. Orton, *The Story of Semiconductors*. Oxford University Press, Feb. 2009.

[2] J. W. T. James W. Cooley, "An algorithm for the machine calculation of complex Fourier series," *Math. Comput.*, vol. 19, pp. 297–301, 1965.

[3] H. F. Harmuth, "On the transmission of information by orthogonal time functions," *AIEE Transactions, Part I: Communication and Electronics*, vol. 79, no. 3, pp. 248–255, July 1960.

[4] R. W. Chang, "Synthesis of band-limited orthogonal signals for multichannel data transmission," *Bell System Technical Journal*, vol. 45, pp. 1775–1796, Dec. 1966.

[5] B. Saltzberg, "Performance of an efficient parallel data transmission system," *IEEE Transactions on Communication Technology*, vol. 15, no. 6, pp. 805–811, Dec. 1967.

[6] R. Chang and R. Gibby, "A theoretical study of performance of an orthogonal multiplexing data transmission scheme," *IEEE Transactions on Communication Technology*, vol. 16, no. 4, pp. 529–540, Aug. 1968.

[7] S. Weinstein and P. Ebert, "Data transmission by frequency-division multiplexing using the discrete fourier transform," *IEEE Transactions on Communication Technology*, vol. 19, no. 5, pp. 628–634, Oct. 1971.

[8] G. Stuber, J. Barry, S. McLaughlin, Y. Li, M. Ingram, and T. Pratt, "Broadband MIMO-OFDM wireless communications," *Proceedings of the IEEE*, vol. 92, no. 2, pp. 271–294, Feb. 2004.

[9] *Radio Broadcasting Systems; Digital Audio Broadcasting (DAB) to mobile, portable and fixed receivers*, ETSI - European Telecommunications Standards Institute EN 300 401 Std., Rev. 1.4.1, Aug. 2006.

[10] *Digital Video Broadcasting (DVB); Frame structure channel coding and modulation for a second generation digital terrestrial television broadcasting system (DVB-T2)*, ETSI - European Telecommunications Standards Institute EN 302 755 Std., Apr. 2012.

[11] *Very high speed digital subscriber line transceivers 2 (VDSL2)*, ITU - International Telecommunication Union - T G.993.2 Std., Dec. 2011.

[12] *IEEE Standard for Broadband over Power Line Networks: Medium Access Control and Physical Layer Specifications*, IEEE 1901 Std., 2010.

[13] *IEEE Standard for Information technology-Telecommunications and information exchange between systems Local and metropolitan area networks-Specific requirements Part 11: Wireless LAN Medium Access Control (MAC) and Physical Layer (PHY) Specifications*, IEEE 802.11 Std., 2012.

[14] *IEEE Standard for Air Interface for Broadband Wireless Access Systems*, IEEE 802.16 Std., 2012.

[15] *3rd Generation Partnership Project; Technical Specification Group Radio Access Network; Evolved Universal Terrestrial Radio Access (E-UTRA); Physical Channels and Modulation (Release 11)* , 3GPP TS 36.211 Std., Rev. 11.1.0, Dec. 2012.

[16] *IEEE Standard for Information Technology-Telecommunications and information exchange between systems Wireless Regional Area Networks (WRAN)-Specific requirements Part 22: Cognitive Wireless RAN Medium Access Control (MAC) and Physical Layer (PHY) Specifications: Policies and Procedures for Operation in the TV Bands*, IEEE 802.22 Std., 2011.

[17] Y. Huang and B. Rao, "On using a priori channel statistics for cyclic prefix optimization in ofdm," in *2011 IEEE Wireless Communications and Networking Conference (WCNC)*, March, pp. 1460–1465.

[18] A. Tonello, S. D"Alessandro, and L. Lampe, "Cyclic Prefix Design and Allocation in Bit-Loaded OFDM over Power Line Communication Channels," *IEEE Transactions on Communications*, vol. 58, no. 11, pp. 3265–3276, Nov.

[19] Z. Zhao-yang and L. Li-Feng, "A novel OFDM transmission scheme with length-adaptive cyclic prefix," *Journal of Zhejiang University SCIENCE*, vol. 5, pp. 1336–1342, 2004.

[20] A. Sahin and H. Arslan, "Multi-user aware frame structure for ofdma based system," in *2012 IEEE Vehicular Technology Conference (VTC Fall)*, Sep., pp. 1–5.

[21] S. Das, E. De Carvalho, and R. Prasad, "Dynamically adaptive bandwidth for sub carriers in ofdm based wireless systems," in *IEEE Wireless Communications and Networking Conference (WCNC 2007)*, March, pp. 1378–1383.

[22] E. Guvenkaya, A. Sahin, and H. Arslan, "Interference visualization and identification for ofdm based systems," in *submitted to 2013 IEEE International Conference on Communications (ICC)*, May 2013, pp. 1–5.

[23] E. Guvenkaya and H. Arslan, "Frequency Domain Eye Diagram for Orthogonal Frequency-Division Multiplexing," in *Proc. Wireless Innovation Forum Conference on Communications Technologies and Software Defined Radio (SDR - WInnComm)*, Washington, DC, Jan. 2013.

[24] A. Sahin, E. Guvenkaya, and H. Arslan, "User distance distribution for overlapping and coexisting cell scenarios," *IEEE Wireless Communications Letters*, vol. 1, no. 5, pp. 432–435, Oct.

[25] J. G. Proakis and M. Salehi, *Digital Communications*, 5th ed. New York: McGraw-Hill, 2008.

[26] J. van de Beek, M. Sandell, and P. Borjesson, "ML estimation of time and frequency offset in OFDM systems," *IEEE Transactions on Signal Processing*, vol. 45, no. 7, pp. 1800–1805, July 1997.

[27] P. Moose, "A technique for orthogonal frequency division multiplexing frequency offset correction," *IEEE Transactions on Communications*, vol. 42, no. 10, pp. 2908–2914, Oct. 1994.

[28] T. Schmidl and D. Cox, "Robust frequency and timing synchronization for OFDM," *IEEE Transactions on Communications*, vol. 45, no. 12, pp. 1613–1621, Dec. 1997.

[29] L. Smaini, *RF Analog Impairments Modeling for Communication Systems Simulation: Application to OFDM-based Transceivers*. Wiley, 2012.

[30] A. Saleh, "Frequency-Independent and Frequency-Dependent Nonlinear Models of TWT Amplifiers," *IEEE Transactions on Communications*, vol. 29, no. 11, pp. 1715–1720, Nov. 1981.

[31] S. H. Han and J. H. Lee, "An overview of peak-to-average power ratio reduction techniques for multicarrier transmission," *IEEE Wireless Communications Mag.*, vol. 12, no. 2, pp. 56–65, Apr. 2005.

[32] S. Brandes, I. Cosovic, and M. Schnell, "Reduction of out-of-band radiation in OFDM systems by insertion of cancellation carriers," *IEEE Commun. Lett.*, vol. 10, no. 6, pp. 420–422, Jun. 2006.

[33] I. Cosovic, S. Brandes, and M. Schnell, "Subcarrier weighting: a method for sidelobe suppression in OFDM systems," *IEEE Commun. Lett.*, vol. 10, no. 6, pp. 444–446, Jun. 2006.

[34] I. Cosovic and T. Mazzoni, "Suppression of sidelobes in OFDM systems by multiple-choice sequences," *Eur. Trans. Telecomms.*, vol. 17, pp. 623–630, 2006.

[35] H. Mahmoud and H. Arslan, "Sidelobe suppression in OFDM-based spectrum sharing systems using adaptive symbol transition," *IEEE Commun. Lett.*, vol. 12, no. 2, pp. 133–135, Feb. 2008.

[36] J. van de Beek and F. Berggren, "N-continuous OFDM," *IEEE Commun. Lett.*, vol. 13, no. 1, pp. 1–3, Jan. 2009.

[37] J. Zhang, X. Huang, A. Cantoni, and Y. Guo, "Sidelobe Suppression with Orthogonal Projection for Multicarrier Systems," *IEEE Trans. Commun.*, vol. 60, no. 2, pp. 589–599, Feb. 2012.

[38] T. Weiss, J. Hillenbrand, A. Krohn, and F. Jondral, "Mutual Interference in OFDM-Based Spectrum Pooling Systems," in *Proc. IEEE Vehicular Technology Conference (VTC)*, vol. 4, May 2004, pp. 1873–1877.

[39] S. Chen and C. Zhu, "ICI and ISI analysis and mitigation for OFDM systems with insufficient cyclic prefix in time-varying channels," *IEEE Trans, Consum. Electron.*, vol. 50, no. 1, pp. 78–83, Feb. 2004.

[40] J. Li and M. Kavehrad, "Effects of time selective multipath fading on OFDM systems for broadband mobile applications," *IEEE Communications Letters*, vol. 3, no. 12, pp. 332–334, Dec. 1999.

[41] H. Steendam and M. Moeneclaey, "Analysis and optimization of the performance of OFDM on frequency-selective time-selective fading channels," *IEEE Trans. Commun.*, vol. 47, no. 12, pp. 1811–1819, Dec. 1999.

[42] H.-C. Wu, "Analysis and characterization of intercarrier and interblock interferences for wireless mobile OFDM systems," *IEEE Trans. Broadcast.*, vol. 52, no. 2, pp. 203–210, Jun. 2006.

[43] E. Bala and L. Cimini, "On the uplink synchronization of OFDMA systems," in *Proc. IEEE MILCOM*, Oct. 2005, pp. 1133–1139 Vol. 2.

[44] W. C. Jakes, Ed., *Microwave mobile communications.* New York: Wiley, June 1974.

[45] "Rec. ITU-R M.1225: Guidelines for Evaluation of Radio Transmission Technologies for IMT-2000," International Telecommunication Union, Tech. Rep., 1997.

[46] Y. Li and J. Cimini, L.J., "Bounds on the interchannel interference of OFDM in time-varying impairments," *IEEE Trans. Commun.*, vol. 49, no. 3, pp. 401–404, Mar. 2001.

[47] J. Cimini, L., "Analysis and simulation of a digital mobile channel using orthogonal frequency division multiplexing," *IEEE Trans. Commun.*, vol. 33, no. 7, pp. 665–675, Jul. 1985.

[48] T. Weiss and F. Jondral, "Spectrum pooling: an innovative strategy for the enhancement of spectrum efficiency," *IEEE Communications Magazine*, vol. 42, no. 3, pp. S8 – 14, mar 2004.

[49] R. Lucky, J. Salz, and E. Weldon, *Principles of data communication.* McGraw-Hill, 1968.

[50] W. McGee, "Eye Pattern for the Binary Noncoherent Receiver," *IEEE Trans. Commun. Technol.*, vol. 19, no. 5, pp. 634 – 643, Oct. 1971.

[51] T. S. Rappaport, *Wireless Communications: Principles and Practice (2nd Edition).* Prentice Hall, 2002.

[52] D. Mugler, "The Centered Discrete Fourier Transform and a parallel implementation of the FFT," in *Acoustics, Speech and Signal Processing (ICASSP), 2011 IEEE International Conference on*, 2011, pp. 1725–1728.

APPENDICES

Appendix A: Acronyms

3G	third generation
3GPP	3rd Generation Partnership Project
4G	fourth generation
ACI	adjacent channel interference
ADSL	asymmetric digital subscriber line
AWGN	additive white Gaussian noise
BER	bit error rate
BPL	Broadband over Power Line
CCDF	complementary cumulative distribution function
CDMA	code division multiple access
CFO	carrier frequency offset
CFR	channel frequency response
CP	cyclic prefix
CR	cognitive radio
DAB	Digital Audio Broadcasting
DFT	discrete Fourier transform
DTFT	discrete-time Fourier transform
DVB-T2	Terrestrial Digital Video Broadcasting
E-UTRA	Evolved Universal Terrestrial Radio Access
FDE	frequency domain equalization
FDED	frequency domain eye diagram
FIR	finite impulse response
GSM	Global System for Mobile Communications
IBO	input back-off

Appendix A (Continued)

IEEE	Institute of Electrical and Electronics Engineers
ICI	inter-carrier interference
IDFT	inverse discrete Fourier transform
i.i.d.	independent and identically distributed
ISI	inter-symbol interference
LAN	local area network
LTE	Long Term Evolution
MIMO	multiple input-multiple output
NBI	narrow band interference
OFDM	orthogonal frequency-division multiplexing
PAPR	peak-to-average power ratio
PHY	physical layer
PSK	phase-shift keying
QAM	quadrature amplitude modulation
QPSK	quadrature phase-shift keying
RC	raised-cosine
RF	radio frequency
SINR	Signal to interference plus noise ratio
SNR	signal-to-noise ratio
TDE	time domain equalization
VDSL2	Very-high-speed digital subscriber line 2
VSA	vector signal analyzer
VSG	vector signal generator
WiMAX	Worldwide Interoperability for Microwave Access
WLAN	wireless local area network
ZP	zero padding